

THS

This is to certify that the thesis entitled

Analysis of the Spectrum of the Single Integral Equation for Scattering from Dielectric Objects

presented by

Jun Yuan

has been accepted towards fulfillment of the requirements for the

M.S. degree in Electric

Electrical and Computer Engineering

Major Professor's Signature

Date

MSU is an Affirmative Action/Equal Opportunity Institution

LIBRARY Michigan State University

PLACE IN RETURN BOX to remove this checkout from your record. TO AVOID FINES return on or before date due. MAY BE RECALLED with earlier due date if requested.

| DATE DUE | DATE DUE | DATE DUE |
|----------|----------|----------|
| | | |
| | | |
| | | |
| | | |
| | | |
| | | |
| | | |
| | | |
| | | |
| | | |
| | | |

2/05 p:/CIRC/DateDue.indd-p.1

Analysis of the Spectrum of the Single Integral Equation for Scattering from Dielectric Objects

 $\mathbf{B}\mathbf{y}$

Jun Yuan

A THESIS

Submitted to
Michigan State University
in partial fulfillment of the requirements
for the degree of

MASTER OF SCIENCE

Electrical and Computer Engineering

2006

ABSTRACT

Analysis of the Spectrum of the Single Integral Equation for Scattering from Dielectric Objects

Bv

Jun Yuan

Surface integral equations are widely used to analyze electromagnetic scattering from a dielectric object residing in free space. Methods for analyzing scattering from dielectric bodies have largely relied on either the PMCHWT or the Müller formulations. It is well known that the PMCHWT formulation result in a first kind Fredholm integral equation, is not well-conditioned and leads to slow convergence. The Müller formulation, on the other hand, results in a second-kind integral equation and is well-conditioned as the hyper-singular terms nearly cancel for low-contrast ratios. However, the Müller formulation is not very accurate for very high-contrast materials. Alternatively, it has been shown that scattering from a dielectric body can be computed using a single unknown and a set of cascaded equations, viz., the single integral equation (SIE) [1]. Existing literature [2] has reported that the condition number of the impedance matrix is excellent. However, no work has been attempted to analyze the convergence and uniqueness of the SIE operator. In this thesis, a detailed analysis is carried out to reveal the underlying mathematical properties of the operator. It will be shown that this operator does not produce unique solutions at internal resonance frequencies. Nonetheless, we suggest a method to overcome spurious resonances and propose an integral equation that is accurate for arbitrary material contrast ratios, while still preserving its well-conditioned nature.

To My Parents

ACKNOWLEDGMENTS

In finishing this research, I have profited intellectually from the support, comments and suggestions of my professors, my colleagues and my friends.

First, I would like to highlight the role of Prof. Shanker Balasubramaniam for being my major advisor, who helped me with his technical knowledge, timely guidance and constant encouragement. I am grateful to Dr. Gregory Kobidze for his instrumental discussions with me on the regular basis. Thanks to Prof. Dennis Nyquist for his review of my presentation in the EM seminar series. I would also like to express my sincere thanks to Prof. Edward Rothwell for consolidating my background knowledge and theory in advanced EM research. Many valuable suggestions from Prof. Leo Kempel have greatly contributed to my research publications.

I would also like to thank my friends and fellow graduate students Chuan Lu, Jun Gao, Jorge Villa, and Pedro Barba for their frequent help in the my study and research on this thesis. Without your comments, I wouldn't have been able to grasp all the materials in such an efficient manner.

Many thanks are also given to Brad Perry for providing me with the LATEX style files that made the writing of the thesis an enjoyable work.

Most of all I would like to thank my parents for their support and education through all levels of my studies. Your recognition and pride in your son has made all this possible.

TABLE OF CONTENTS

| LIST O | F FIGURES | vi |
|---------------------|---|------|
| KEY T | O SYMBOLS AND ABBREVIATIONS | viii |
| CHAPT Introdu | TER 1 | 1 |
| CHAPT Integral | TER 2 Equations for Scattering from Dielectric bodies | 3 |
| 2.1 | Definition of the dielectric scattering problem | 3 |
| 2.2 | Surface Equivalence Theorem | 3 |
| 2.3 | Single Integral Equation | 6 |
| СНАРТ | TER 3 | |
| Numerio | cal Solution using the Method of Moments | 12 |
| 3.1 | Method of Moments | 12 |
| 3.2 | Current Basis Functions | 14 |
| 3.3 | Projection and Inner Product | 15 |
| 3.4 | Construction of the Moment-Method Matrix | 17 |
| 3.5 | Augmenting with the Fast Multipole Method | 19 |
| 3.6 | Numerical Results | 20 |
| CHAPT Spectra | TER 4 l Analysis of the SIE Operator | 31 |
| 4.1 | Definition of the Spectrum Analysis | 31 |
| 4.2 | Spectrum Properties of the Integral Operators | 35 |
| 4.3 | Analysis of the SIE Spectrum | 37 |
| 4.4 | Well-behaved CSIE Operator | 39 |
| 4.5 | An alternative integral equation scheme | 41 |
| 4.6 | Implementation and solution of the augmented integral equations | 47 |
| CHAPT Conclus | TER 5 ions | 58 |
| APPEN Definition | DIX A on of a second kind integral operator | 61 |
| BIBLIO | GRAPHY | 63 |

LIST OF FIGURES

| Figure 2.1 | Homogeneous dielectric scattering object (ε_2, μ_2) embedded in the medium (ε_1, μ_1) | 10 |
|------------|--|----|
| Figure 2.2 | Equivalence principle models | 10 |
| Figure 2.3 | Equivalence principle models of SIE | 11 |
| Figure 3.1 | Triangulated meshing of a dielectric sphere with $r=1.0$. The number of triangles is 2904, and the number of edges is 4356 | 22 |
| Figure 3.2 | Triangle pair (T_i^+, T_i^-) and parameters associated with the <i>i</i> th edge. | 23 |
| Figure 3.3 | Geometry parameters of the triangle pair $T_{\mathbf{i}}^+$ and $T_{\mathbf{i}}^-$ | 24 |
| Figure 3.4 | RCS pattern of an $\varepsilon_2 = 2\varepsilon_0$ sphere in the x-y plane at $f_0 = 160 \mathrm{MHz}$. | 25 |
| Figure 3.5 | RCS pattern of an $\varepsilon_2 = 4\varepsilon_0$ sphere in the x-y plane at $f_0 = 160 \mathrm{MHz}$. | 26 |
| Figure 3.6 | RCS pattern of an $\varepsilon_2 = 4\varepsilon_0$ sphere in the x-y plane at $f_0 = 225 \mathrm{MHz}$. | 27 |
| Figure 3.7 | RCS pattern of an $\varepsilon_2=4\varepsilon_0$ sphere in the x-y plane at $f_0=300 \mathrm{MHz}$. | 28 |
| Figure 3.8 | RCS pattern of an $\varepsilon_2 = 4\varepsilon_0$ cubic box in the x-y plane at $f_0 = 257 \text{MHz}$ | 29 |
| Figure 3.9 | RCS pattern of a fat almond in the x - y plane at $f_0 = 100 \mathrm{MHz}$ | 30 |
| Figure 4.1 | Plot of three spectral functions of $\lambda_{T, X}^n$ for $k_1 a \in [0.01, 6]$, and $n \in [1, 3, 5]$ | 49 |
| Figure 4.2 | Plot of three spectral functions of $\lambda_{\mathrm{T,\ U}}^{\mathrm{n}}$ for $k_1a\in[0.01,6]$, and $n\in[1,3,5]$ | 50 |
| Figure 4.3 | Plot of three spectral functions of $\lambda_{K^+,X}^n$ for $k_1a \in [0.01, 6]$, and $n \in [1,3,5]$ | 51 |
| Figure 4.4 | Plot of three spectral functions of $\lambda_{K^+,U}^n$ for $k_1a \in [0.01, 6]$, and $n \in [1, 3, 5]$ | 52 |
| Figure 4.5 | Plot of three spectral functions of $\lambda_{K,X}^n$ for $k_1a \in [0.01, 6]$, and | 53 |
| Figure 4.6 | $n \in [1,3,5]$ | აა |
| rigure 4.0 | Plot of three spectral functions of $\lambda_{K^-,U}^n$ for $k_1a \in [0.01, 6]$, and $n \in [1, 3, 5]$ | 54 |
| Figure 4.7 | | 55 |
| Diames 4.0 | | 00 |
| Figure 4.8 | Plot of three spectral functions of $\lambda_{\mathbf{Sm}, \mathbf{X}}^{\mathbf{n}}$ for $k_1 a \in [0.01, 6], \frac{\varepsilon_2}{\varepsilon_1} = 4.0$ and $n \in [2, 3, 5], \dots$ | 56 |

| Figure 4.9 | Plot of three spectral functions of $\lambda_{\mathbf{Sm}}^{\mathbf{n}}$, U for $k_1 a \in [0.01, 6]$, $\frac{\varepsilon_2}{\varepsilon_1} =$ | |
|------------|--|----|
| | $4.0 \text{ and } n \in [2, 3, 5].$ | 57 |

KEY TO SYMBOLS AND ABBREVIATIONS

CEM: Computational Electromagnetics

MoM: Method of Moment

EFIE: Electric Field Integral Equation

MFIE: Magnetic Field Integral Equation

CFIE: Combined Field Integral Equation

PMCHWT: Poggio-Miller-Chang-Harrington-Wu-Tai

SIE: Single Integral Equation

FMM: Fast Multipole Method

CSIE: Combined Source Integral Equation

ASIE: Augmented Single Integral Equation

CHAPTER 1

INTRODUCTION

Analysis of electromagnetic scattering from arbitrary shaped three-dimensional (3-D) homogeneous or layered homogeneous dielectric bodies is of considerable interest and is largely motivated by possible application in the society of computational electromagetics, due to the wide application of materials in a variety of radar targets. The early studies focused mainly on spherical or nearly spherical scatterers by using classical analysis. But in many applications the scatterer is an arbitrarily shaped 3-D object. For dielectric objects with a surface of arbitrary shape, one has to resort to some approximate numerical techniques based on either integral or differential equations. Recent developments in the field of computational electromagnetics (CEM) have greatly expanded the palette of analysis tools to include problems in which the boundary conditions or the shape of the scatterer makes previous classical mathematical approaches intractable. Surface integral equations are often preferred for homogeneous or layered homogeneous objects, as they permit the use of surface equivalent currents. Compared with volume integral equations, the computational cost is greatly reduced from $\mathcal{O}(N^3)$ to $\mathcal{O}(N^2)$.

However, the efficiency of this method depends heavily on the mathematical formulation. Given the fact that the CEM engineers need to solve practical problems of millions of unknowns, it is essential that the formulation yield a well-conditioned matrix system, so that the solution can converge to an accurate result rapidly. On the other hand, the formulation should yield a unique solution. In other words, the mathematical model should produce unique results at all frequencies.

An overview of the mathematic models for analyzing the EM scattering from a dielectric body of arbitrary shape is given in Chapter 2, including a description of different integral equation approaches with an emphasis on the single integral equation (SIE) formulation.

Chapter 3 covers the MoM implementation of the SIE scheme. Details of the method are elaborated upon, especially, the basis functions used, and the method to compute the inner product with the testing function. Also covered in Chapter 3 is the adaptation of the FMM algorithm for this specific scenario. Numerical results are illustrated at the end of this chapter, and these results are compared against the solutions obtained either using the classic approach or using an extant numerical code developed by Dr. Shanker Balasubramaniam at Michigan State University.

The spectral analysis of integral equation operator is introduced in Chapter 4. The convergence properties of various equations are explained and illustrated in this chapter. The spectrum of the peculiar SIE operator is investigated from the mathematic perspective. As will be shown, the SIE operator does not yield unique solutions at resonance frequencies. Hence, we proceed to devise an augmented SIE operator and prove its validity thereafter.

Chapter 5 serves to conclude this thesis. Contributions to this research are discussed, along with future work necessary to expand the applicability of this new scheme in handling the EM scattering phenomena.

CHAPTER 2

INTEGRAL EQUATIONS FOR SCATTERING FROM DIELECTRIC BODIES

2.1 Definition of the dielectric scattering problem

Consider a homogeneous dielectric body of volume V, as shown in Figure 2.1, whose boundary is denoted by Ω . Additionally, Ω^+ and Ω^- denote surfaces that are conformal to and lie just outside and inside Ω , and $\hat{\mathbf{n}}$ denotes the outward pointing normal to Ω . The regions inside (denoted as R_1) and outside (denoted as R_2) Ω are characterized by material parameters (ε_1, μ_1) and (ε_2, μ_2) , respectively. Impressed sources residing within R_1 produce incident electromagnetic fields electric and magnetic fields $\left\{\mathbf{E}^{\mathrm{inc}}, \mathbf{H}^{\mathrm{inc}}\right\}$. The interaction of the incident fields with Ω gives rise to the scattered fields $\mathbf{E}^{\mathrm{scat}}_1(\mathbf{r}), \mathbf{H}^{\mathrm{scat}}_1(\mathbf{r})$. The total fields $\left\{\mathbf{E}^{\mathrm{tot}}, \mathbf{H}^{\mathrm{tot}}_1\right\}$ in R_1 comprise both the incident and scattered fields, viz.,

$$\mathbf{E}_{1}^{\text{tot}}(\mathbf{r}) = \mathbf{E}^{\text{inc}}(\mathbf{r}) + \mathbf{E}_{1}^{\text{scat}}(\mathbf{r})$$
 (2.1a)

$$\mathbf{H}_{1}^{\text{tot}}(\mathbf{r}) = \mathbf{H}^{\text{inc}}(\mathbf{r}) + \mathbf{H}_{1}^{\text{scat}}(\mathbf{r})$$
 (2.1b)

Inside Ω , the fields are expressed by $\mathbf{E}_2^{\mathrm{scat}}(\mathbf{r}), \mathbf{H}_2^{\mathrm{scat}}(\mathbf{r})$.

2.2 Surface Equivalence Theorem

The equivalence principle [1] is applied to the scattering problem from a dielectric body, as illustrated by Figure 2.2. One can set up a problem equivalent to the original problem external to Ω as follows. Let the original field exist external to Ω , and the null field internal to Ω , while the whole region is characterized by (ε_1, μ_1) . This is shown in Figure 2.2(a). To support the scattered field, there must exist surface

currents J_1 , M_1 on Ω according to the continuity conditions across the boundary. The currents therefore satisfy the constraints

$$\mathbf{J}_1 = \hat{\mathbf{n}} \times [\mathbf{H}^{\text{inc}} + \mathbf{H}_1^{\text{scat}}] \tag{2.2a}$$

$$\mathbf{M}_1 = [\mathbf{E}^{\text{inc}} + \mathbf{E}_1^{\text{scat}}] \times \hat{\mathbf{n}}$$
 (2.2b)

where $\hat{\mathbf{n}}$ is an outward pointing normal. Since the currents radiate in unbounded homogenous space, we can determine the scattered field using

$$\mathbf{E}_1^{\text{scat}}(\mathbf{r}) = \eta_1 \mathbf{L}_1(\mathbf{J}_1) - \mathbf{K}_1(\mathbf{M}_1) \tag{2.3a}$$

$$\mathbf{H}_{1}^{\text{scat}}(\mathbf{r}) = \mathbf{K}_{1}(\mathbf{J}_{1}) + \eta_{1}^{-1}\mathbf{L}_{1}(\mathbf{M}_{1})$$
 (2.3b)

where

$$\mathbf{L}_{1}\{\mathbf{X}\} \doteq -jk_{1} \int_{\Omega} \left[\bar{\bar{I}} + \frac{1}{k_{1}^{2}} \nabla \nabla \right] G_{1}(\mathbf{r}, \mathbf{r}') \cdot \mathbf{X}(\mathbf{r}') \ dS'$$
 (2.4a)

$$\mathbf{K}_{1}\{\mathbf{X}\} \doteq \int_{\Omega} \nabla \times \left[\mathbf{X}(\mathbf{r}')G_{1}(\mathbf{r}, \mathbf{r}')\right] dS'$$
 (2.4b)

 $ar{ar{I}}$ is the idem factor, or unit dyad.

Similarly, we can set up another equivalence for the field internal to Ω as shown in Figure 2.2(b). Another set of equivalent currents J_2 , M_2 , prescribed by

$$\mathbf{J_2} = -\hat{\mathbf{n}} \times \mathbf{H}_2^{\text{scat}} \tag{2.5a}$$

$$\mathbf{M}_2 = -\mathbf{E}_2^{\mathrm{scat}} \times \hat{\mathbf{n}} \tag{2.5b}$$

reside over Ω in the homogeneous space of (ε_2, μ_2) , and produce the null field external

to Ω and the original field $\mathbf{E}_2^{\mathrm{scat}}(\mathbf{r}), \mathbf{H}_2^{\mathrm{scat}}(\mathbf{r})$ internal to Ω , which is determined as

$$\mathbf{E}_2^{\text{scat}}(\mathbf{r}) = \eta_2 \mathbf{L}_2 \{ \mathbf{J}_2 \} - \mathbf{K}_2 \{ \mathbf{M}_2 \}$$
 (2.6a)

$$\mathbf{H}_{2}^{\text{scat}}(\mathbf{r}) = \mathbf{K}_{2}\{\mathbf{J}_{2}\} + \eta_{2}^{-1}\mathbf{L}_{2}\{\mathbf{M}_{2}\}$$
 (2.6b)

Our specification of the null field internal/external to Ω is overly restrictive in the preceding models. Any other field would serve equally well, given that the resulting equivalent currents satisfy the field continuity constraints. Yet, our proposed choices prescribe the complementary relation between the currents in Figure 2.2(a) and Figure 2.2(b), viz.,

$$\mathbf{J}_1 = \hat{\mathbf{n}} \times [\mathbf{H}^{\text{inc}} + \mathbf{H}_1^{\text{scat}}] = (-\hat{\mathbf{n}}_2) \times \mathbf{H}_2^{\text{scat}} = -\mathbf{J}_2 \tag{2.7a}$$

$$\mathbf{M}_1 = [\mathbf{E}^{\text{inc}} + \mathbf{E}_1^{\text{scat}}] \times \hat{\mathbf{n}} = \mathbf{E}_2^{\text{scat}} \times (-\hat{\mathbf{n}}_2) = -\mathbf{M}_2$$
 (2.7b)

due to the fact that

$$\hat{\mathbf{n}} \times [\mathbf{H}^{\text{inc}} + \mathbf{H}_1^{\text{scat}}] = \hat{\mathbf{n}} \times \mathbf{H}_2^{\text{scat}}$$
 (2.8a)

$$\hat{\mathbf{n}} \times [\mathbf{E}^{\text{inc}} + \mathbf{E}_1^{\text{scat}}] = \hat{\mathbf{n}} \times \mathbf{E}_2^{\text{scat}}$$
 (2.8b)

and

$$\hat{\mathbf{n}}_2 = -\hat{\mathbf{n}} \tag{2.9}$$

is the normal vector inward to Ω .

Using Eqs. [2.3 - 2.6], the classical Poggio-Miller-Chang-Harrington-Wu-Tai (PM-CHWT) formulation [2] is derived, leading to

$$\hat{\mathbf{n}} \times \mathbf{E}^{\text{inc}}|_{\Omega^{+}} = -\hat{\mathbf{n}} \times \mathbf{E}_{1}^{\text{scat}}|_{\Omega^{+}} + \hat{\mathbf{n}} \times \mathbf{E}_{2}^{\text{scat}}|_{\Omega^{-}}$$
(2.10a)

$$\hat{\mathbf{n}} \times \mathbf{H}^{\text{inc}}|_{\Omega^{+}} = -\hat{\mathbf{n}} \times \mathbf{H}_{1}^{\text{scat}}|_{\Omega^{+}} + \hat{\mathbf{n}} \times \mathbf{H}_{2}^{\text{scat}}|_{\Omega^{-}}$$
 (2.10b)

An alternate approach suggested by Müller [3] is to scale the interior and exterior field operators by the constitutive parameters and then subtract eqs. 2.5 from eqs. 2.2, representing the interior and exterior problems, respectively. The Müller equations read as

$$-\hat{\mathbf{n}} \times \mathbf{E}^{\mathrm{inc}}|_{\Omega^{+}} = (1+\alpha) \,\mathbf{M}_{1} + \hat{\mathbf{n}} \times (\mathbf{E}_{1}^{\mathrm{scat}}|_{\Omega^{+}} - \alpha \mathbf{E}_{2}^{\mathrm{scat}}|_{\Omega^{-}}) \tag{2.11a}$$

$$-\hat{\mathbf{n}} \times \mathbf{H}^{\text{inc}}|_{\Omega^{+}} = -(1+\beta)\mathbf{J}_{1} + \hat{\mathbf{n}} \times (\mathbf{H}_{1}^{\text{scat}}|_{\Omega^{+}} + \beta \mathbf{H}_{2}^{\text{scat}}|_{\Omega^{-}})$$
(2.11b)

where $\alpha = \varepsilon_2/\varepsilon_1$, and $\beta = \mu_2/\mu_1$, as chosen by Müller in his construction of integral equations.

This formulation has some advantages over the PMCHWT formulation for low contrast materials (i.e., $\varepsilon_r < 20$). Specifically: 1) it behaves as a second-kind integral equation; 2) the static terms of the **L**-operator in Eqs. 2.4 cancel in the limit as $|\mathbf{r} - \mathbf{r}'| \to 0$, effectively canceling the hypersingular term [3, pg. 300]; and 3) the Müller formulation has a lower condition number than the PMCHWT formulation for moderate to low contrast materials.

2.3 Single Integral Equation

The coupled vector integral equations, PMCHWT and Müller require one to solve for a set of unknown equivalent electric and magnetic currents. Marx [4] developed, in both the time and frequency domains, a single integral equation for scattering problems involving homogeneous dielectric bodies. Glisson [5] elaborated upon the technique for 3-D dielectric objects in the frequency domain using the techniques and terms that EM researchers are more familiar with. Numerical demonstration was recently reported by Yeung [6] and Tsang [7].

To determine the scattered field using SIE, we employ the equivalence principle to develop two different models. For the same original problem, two models equivalent in the external and internal regions, are illustrated in Figure 2.3. A model equivalent to the exterior region is shown in Figure 2.3(a). In contrast to the classical model in Figure 2.2(a), only a single current \mathbf{J}_{eff} resides in the homogeneous medium (ε_1, μ_1) to produce the correct scattered field external to Ω . The equivalent source \mathbf{J}_{eff} , however, is not unique unless the scattered field is specified internal to Ω . In the approach usually followed, the auxiliary field is set to $\mathbf{0}$. And \mathbf{J}_{eff} is uniquely determined by

$$\begin{aligned} \mathbf{J}_{\text{eff}} &= \hat{\mathbf{n}} \times [\mathbf{H}^{\text{inc}} + \mathbf{H}_{1}^{\text{scat}}(\mathbf{J}_{\text{eff}}, \mathbf{0})] \\ &= \hat{\mathbf{n}} \times \mathbf{H}^{\text{inc}} + \hat{\mathbf{n}} \times \mathbf{K}_{1} \{ \mathbf{J}_{\text{eff}} \} \end{aligned}$$
(2.12)

Equivalence to the original problem inside Ω (Figure 2.3(b)), the sources are constructed by imposing $(\mathbf{J}_2, \mathbf{M}_2)$. These sources radiate in a homogeneous medium (ε_2, μ_2) and produce the correct scattered field inside Ω and a null field outside Ω . Continuity of the true field is enforced to relate the equivalent currents \mathbf{J}_{eff} and $(\mathbf{J}_2, \mathbf{M}_2)$ using the relations,

$$\hat{\mathbf{n}} \times \hat{\mathbf{n}} \times \mathbf{E}_2^{\text{scat}} = \hat{\mathbf{n}} \times \hat{\mathbf{n}} \times [\mathbf{E}^{\text{inc}} + \mathbf{E}_1^{\text{scat}}]$$
 (2.13)

$$\hat{\mathbf{n}} \times \mathbf{H}_2^{\text{scat}} = \hat{\mathbf{n}} \times [\mathbf{H}^{\text{inc}} + \mathbf{H}_1^{\text{scat}}] \tag{2.14}$$

Thus,

$$\mathbf{J}_{2} = -\hat{\mathbf{n}} \times \mathbf{H}_{2}^{\text{scat}} \big|_{\Omega^{+}}
= -\hat{\mathbf{n}} \times [\mathbf{H}^{\text{inc}} + \mathbf{H}_{1}^{\text{scat}}] \big|_{\Omega^{+}}
= -\hat{\mathbf{n}} \times \mathbf{H}^{\text{inc}} - \hat{\mathbf{n}} \times \mathbf{K}_{1} \{ \mathbf{J}_{\text{eff}} \} \big|_{\Omega^{+}}$$
(2.15)

$$\begin{aligned} \mathbf{M}_{2} &= -\mathbf{E}_{2}^{\text{scat}} \times \hat{\mathbf{n}} \big|_{\Omega^{+}} \\ &= -[\mathbf{E}^{\text{inc}} + \mathbf{E}_{1}^{\text{scat}}] \times \hat{\mathbf{n}} \big|_{\Omega^{+}} \\ &= -\mathbf{E}^{\text{inc}} \times \hat{\mathbf{n}} - \eta_{1} \mathbf{L}_{1} \{ \mathbf{J}_{\text{eff}} \} \times \hat{\mathbf{n}} \big|_{\Omega^{+}} \end{aligned}$$
(2.16)

We may restate Eqs. 2.13 and 4.28 in terms of $J_{\rm eff}$ as

$$\hat{\mathbf{n}} \times \hat{\mathbf{n}} \times \mathbf{E}^{\text{inc}} = \hat{\mathbf{n}} \times \hat{\mathbf{n}} \times (\eta_2 \mathbf{L}_2 \{ \mathbf{J}_2 \} - \mathbf{K}_2 \{ \mathbf{M}_2 \} - \eta_1 \mathbf{L}_1 \{ \mathbf{J}_{\text{eff}} \})
= \hat{\mathbf{n}} \times \hat{\mathbf{n}} \times (\eta_2 \mathbf{L}_2 \{ -\hat{\mathbf{n}} \times \mathbf{H}^{\text{inc}} - \hat{\mathbf{n}} \times \mathbf{K}_1 \{ \mathbf{J}_{\text{eff}} \} \}
- \mathbf{K}_2 \{ -\mathbf{E}^{\text{inc}} \times \hat{\mathbf{n}} - \eta_1 \mathbf{L}_1 \{ \mathbf{J}_{\text{eff}} \} \times \hat{\mathbf{n}} \}
- \eta_1 \mathbf{L}_1 \{ \mathbf{J}_{\text{eff}} \})$$
(2.17)

$$\hat{\mathbf{n}} \times \mathbf{H}^{\text{inc}} = \hat{\mathbf{n}} \times (\frac{1}{\eta_2} \mathbf{L}_2 \{ \mathbf{M}_2 \} + \mathbf{K}_2 \{ \mathbf{J}_2 \} - \mathbf{K}_1 \{ \mathbf{J}_{\text{eff}} \})$$

$$= \hat{\mathbf{n}} \times \left(\frac{1}{\eta_2} \mathbf{L}_2 \{ -\mathbf{E}^{\text{inc}} \times \hat{\mathbf{n}} - \eta_1 \mathbf{L}_1 \{ \mathbf{J}_{\text{eff}} \} \times \hat{\mathbf{n}} \} \right)$$

$$+ \mathbf{K}_2 \{ -\hat{\mathbf{n}} \times \mathbf{H}^{\text{inc}} - \hat{\mathbf{n}} \times \mathbf{K}_1 \{ \mathbf{J}_{\text{eff}} \} \}$$

$$- \mathbf{K}_1 \{ \mathbf{J}_{\text{eff}} \})$$

$$(2.18)$$

Rearranging both sides of eqn. 2.17 yields the EFIE equation

$$-\eta_{2}\hat{\mathbf{n}}\times\hat{\mathbf{n}}\times\mathbf{L}_{2}\{\hat{\mathbf{n}}\times\mathbf{K}_{1}\{\mathbf{J}_{eff}\}\}-\eta_{1}\hat{\mathbf{n}}\times\hat{\mathbf{n}}\times\mathbf{K}_{2}\{\hat{\mathbf{n}}\times\mathbf{L}_{1}\{\mathbf{J}_{eff}\}\}-\eta_{1}\hat{\mathbf{n}}\times\hat{\mathbf{n}}\times\mathbf{L}_{1}\{\mathbf{J}_{eff}\}=\mathbf{E}_{rhs}$$
(2.19)

where the term

$$\mathbf{E}_{\mathrm{rhs}} = \hat{\mathbf{n}} \times \hat{\mathbf{n}} \times \mathbf{E}^{\mathrm{inc}} + \eta_2 \hat{\mathbf{n}} \times \hat{\mathbf{n}} \times \mathbf{L}_2 \{ \hat{\mathbf{n}} \times \mathbf{H}^{\mathrm{inc}} - \hat{\mathbf{n}} \times \hat{\mathbf{n}} \times \mathbf{K}_2 \{ \mathbf{E}^{\mathrm{inc}} \times \hat{\mathbf{n}} \} \} \quad (2.20)$$

is the right-hand-side given by the incident field. Similarly, the MFIE equation can be derived, leading to

$$\hat{\mathbf{n}} \times \mathbf{K}_2 \{ \hat{\mathbf{n}} \times \mathbf{K}_1 \{ \mathbf{J}_{eff} \} \} + \frac{\eta_1}{\eta_2} \hat{\mathbf{n}} \times \mathbf{L}_2 \{ \hat{\mathbf{n}} \times \mathbf{L}_1 \{ \mathbf{J}_{eff} \} \} - \hat{\mathbf{n}} \times \mathbf{K}_1 \{ \mathbf{J}_{eff} \} = \mathbf{H}_{rhs} \quad (2.21)$$

where

$$\mathbf{H}_{\text{rhs}} = \hat{\mathbf{n}} \times \mathbf{H}^{\text{inc}} + \hat{\mathbf{n}} \times \mathbf{K}_2 \{ \hat{\mathbf{n}} \times \mathbf{H}^{\text{inc}} \} - \frac{1}{\eta_2} \hat{\mathbf{n}} \times \mathbf{L}_2 \{ \hat{\mathbf{n}} \times \mathbf{E}^{\text{inc}} \}$$
(2.22)

The unknown fields in Eqs. 4.28 and 2.13 can be expressed in terms of integrals over their respective sources. Then Eqs. 2.15 and 2.16 give J_2 and M_2 in terms of the single current $J_{\rm eff}$, and Eqs. 2.19 or 2.21, or an appropriate linear combination of these equations represents an integral equation to be solved for $J_{\rm eff}$.

In the next few chapters, we will investigate the desirable properties of the MFIE equation (in eqn. 2.21). It will be shown that the MFIE equation is a second kind integral operator (Appendix A).

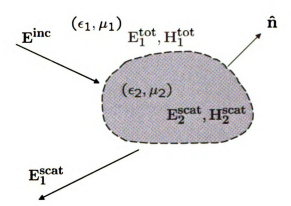


Figure 2.1. Homogeneous dielectric scattering object (ε_2, μ_2) embedded in the medium (ε_1, μ_1) .

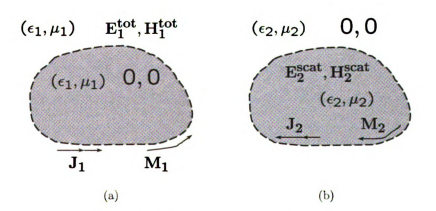


Figure 2.2. Equivalence principle models.

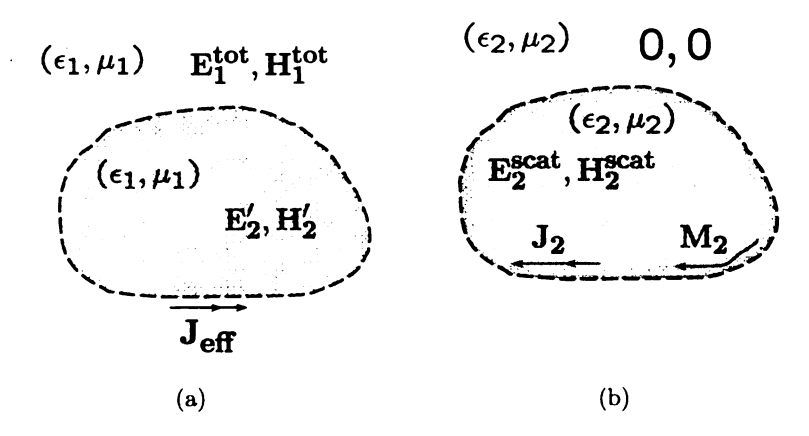


Figure 2.3. Equivalence principle models of SIE.

CHAPTER 3

NUMERICAL SOLUTION USING THE METHOD OF MOMENTS

3.1 Method of Moments

The method of moments is employed to convert the MFIE into a matrix equation, which can be algebraically solved to determine the unknown effective current [8]. The general method of converting a linear integrodifferential equation

$$\mathcal{L}\{f(x)\} = g(x) \tag{3.1}$$

into a matrix equation is discussed here. The first step in converting the integral equation to a matrix equation is to expand the unknown in a finite number of subdomain basis functions

$$f(x) = \sum_{i=1}^{N} a_i f_{B_i}(x)$$
 (3.2)

Inserting this into the general equation and using the linearity of the operator ${\cal L}$ result in

$$\sum_{j=1}^{n} a_{j} \mathcal{L}\{f_{B_{j}}(x)\} = g(x)$$
(3.3)

The next step is to test this equation with a testing function set. The testing procedure is accomplished by taking the inner product of the equation with a testing function. The inner product of two real functions is defined as the integral of their product over their region of support,

$$\langle f(x), h(x) \rangle = \int_{\mathbf{a}}^{\mathbf{b}} f(x) \ h(x) \ dx. \tag{3.4}$$

Using this definition, eqn. 3.3 can be converted into N linear equations by testing it with N different testing functions

$$\sum_{j=1}^{n} \langle f_{T_i}(x), \mathcal{L}f_{B_j}(x) \rangle a_j \cong \langle f_{T_i}(x), g(x) \rangle, \quad i = 1, N$$
(3.5)

The integral equation for the unknown continuous function f(x) has now been converted into a system of N equations in N unknowns. The unknowns now are the coefficients of the basis functions, i.e., a_i . Converting into matrix notation gives

$$\bar{L} \cdot \vec{a} = \vec{g} \tag{3.6}$$

where $\bar{\bar{L}}$ is an $N \times N$ matrix, and \vec{a} and \vec{g} are N-dimensional vectors with elements

$$L_{ij} = \langle f_{Ti}(x), \mathcal{L}f_{Bj}(x) \rangle$$
 (3.7)

and

$$g_{\mathbf{i}} = \langle f_{\mathbf{T}\mathbf{i}}(x), g(x) \rangle.$$
 (3.8)

The matrix \bar{L} can now be inverted provided it is not singular. A necessary condition to ensure a nonsingular matrix is the use of a set of independent basis function. Many choices of basis and testing functions are possible. For this application, the Galerkin testing procedure was chosen. For the Galerkin method, the basis and testing functions are the same, i.e.,

$$g_{\mathbf{i}} = \langle f_{\mathbf{B}\mathbf{i}}(x), g(x) \rangle.$$
 (3.9)

In the specific application of the method of moments to the EFIE, the current on the electrical body is treated as the unknown. This requires the definition of four different types of basis functions, each to be used on a specific portion of the body. These are described in the next section.

3.2 Current Basis Functions

The equation in 2.19 or 2.21 involve a set of cascaded operators, i.e., the output of one operator serves as the feed of another operator. Numerical implementation of the integral equation requires transforming the SIE 2.19 and 2.21 or 2.21 into a matrix equation. To this end, the surface Ω is discretized by a set of triangular patches. Figure 3.1 shows an example of modeling a spherical surface. The mesh tool is developed using MATLAB. The unknown effective current \mathbf{J}_{eff} is expanded in terms of Rao-Wilton-Glisson (RWG) functions [9] associated with an edge i of the triangulated surface. Figure 3.2 shows such a triangle pair. Points in $T_{\mathbf{i}}^+$ are designated by the local position vector $\vec{\rho}_{\mathbf{i}}^+$ pointing from the free vertex $O_{\mathbf{i}}^+$ of $T_{\mathbf{i}}^+$. Similar remarks apply to the position vector $\vec{\rho}_{\mathbf{i}}^-$ in $T_{\mathbf{i}}^-$ except that it is directed toward the free vertex opposite to the edge i in $T_{\mathbf{i}}^-$.

A vector basis function \mathbf{f}_i associated with the *i*th edge is defined as

$$\mathbf{f_{i}}(\mathbf{r}) = \begin{cases} \frac{l_{i}}{2A_{i}^{+}} \vec{\rho_{i}^{+}}, & \mathbf{r} \in T_{i}^{+} \\ \frac{l_{i}}{2A_{i}^{-}} \vec{\rho_{i}^{-}}, & \mathbf{r} \in T_{i}^{-} \\ 0, & \text{otherwise} \end{cases}$$
(3.10)

where l_i is the length of the common edge i and A_i^{\pm} are the areas of the triangles T_i^{\pm} , respectively.

The effective current J_{eff} is thus expanded in terms of f_i

$$\mathbf{J}_{\text{eff}}(\mathbf{r}) = \sum_{i=1}^{n} I_{i}^{\text{eff}} \mathbf{f}_{i}(\mathbf{r})$$
 (3.11)

where N is the total number of edges in the triangular-patch model of Ω and I_i^{eff} are the unknown current coefficients.

The basis function $\mathbf{f_i}$ possesses very desirable properties that are described in [9].

- 1. The current has no component normal to the boundary (which excludes the common edge) of the surface formed by the triangle pair $T_{\mathbf{i}}^{+}$ and $T_{\mathbf{i}}^{-}$, and hence no line charges exist along this boundary.
- 2. The component of current normal to the $i^{\rm th}$ edge is constant and continuous across the edge as may be seen with the aid of Figure 3.3, which shows that the normal component of $\vec{\rho}_{\bf i}^{\pm}$ along edge i is just the height of triangle $T_{\bf i}^{\pm}$ with edge i as the base and the height expressed as $2A_{\bf i}^{\pm}/l_{\bf i}$. This latter factor normalizes ${\bf f}_{\bf i}$ in eqn. 3.10 such that its flux density normal to edge i is unity, ensuring continuity of current normal to the edge. This result, together with 1, implies that all edges of $T_{\bf i}^{\pm}$ and $T_{\bf i}^{\pm}$ free of line charges
- 3. The surface divergence of $\mathbf{f_i}$, which is proportional to the surface charge density associated with the basis element, is

$$\nabla_{\mathbf{s}} \cdot \mathbf{f_i}(\mathbf{r}) = \begin{cases} \frac{l_i}{A_i^+}, & \mathbf{r} \in T_i^+ \\ -\frac{l_i}{A_i^-}, & \mathbf{r} \in T_i^- \\ 0, & \text{otherwise} \end{cases}$$
(3.12)

3.3 Projection and Inner Product

An important issue associated with the cascaded operators in eqn. 2.21 is the choice of intermediate projection spaces for each operator product. If the effective current 3.11 were substituted directly into the single integral equation 2.21, the resulting equation would be difficult to evaluate because of the cascaded integral operator $\hat{\mathbf{n}} \times \mathbf{L}_2\{\hat{\mathbf{n}} \times \mathbf{L}_1\{\star\}\}$, which involves a hyper-singular component attributed to the

differential operator $\nabla\nabla$ in eqn. 2.4. Instead, it is more convenient to expand the arguments of the integral operators in 2.15 and 2.16 using the vector basis function $\mathbf{f_i}$. Hence, 2.15 and 2.16 can be rewritten as

$$-\hat{\mathbf{n}} \times [\mathbf{H}^{\text{inc}} + \mathbf{H}_{1}^{\text{scat}}] \Big|_{\Omega^{+}} = \sum_{i=1}^{n} I_{i}^{e} \mathbf{f}_{i}$$
 (3.13)

$$-[\mathbf{E}^{\mathrm{inc}} + \mathbf{E}_{1}^{\mathrm{scat}}] \times \hat{\mathbf{n}} \big|_{\Omega^{+}} = \sum_{i=1}^{n} I_{i}^{\mathrm{m}} \mathbf{f}_{i}$$
 (3.14)

where $\mathbf{H}_2^{\text{scat}}$ and $\mathbf{E}_2^{\text{scat}}$ are given by eqs. 2.15 and 2.16, and (I_i^e, I_i^m) are the intermediate expansion coefficients.

Employing simple verctor identities, we obtain

$$[\mathbf{H}^{\text{inc}}(\mathbf{r}_{+}) + \mathbf{H}_{1}^{\text{scat}}(\mathbf{r}_{+})] \cdot \mathbf{l}_{i} = \hat{\mathbf{n}} \cdot \left\{ -\hat{\mathbf{n}} \times [\mathbf{H}^{\text{inc}}(\mathbf{r}_{+}) + \mathbf{H}_{1}^{\text{scat}}(\mathbf{r}_{+})] \times \mathbf{l}_{i} \right\}$$

$$= \hat{\mathbf{n}} \cdot \left\{ \sum_{j=1}^{n} I_{j}^{e} \mathbf{f}_{j}(\mathbf{r}) \times \mathbf{l}_{i} \right\}$$

$$= \sum_{j=1}^{n} I_{j}^{e} (\mathbf{l}_{i} \times \hat{\mathbf{n}}) \cdot \mathbf{f}_{j}(\mathbf{r})$$

$$(3.15)$$

where $\mathbf{l_i}$ has been chosen in such a way that if a right-hand screw through the triangle T_i^+ were rotated in the sense of the vector $\mathbf{l_i}$, it would advance in the direction of the unit normal $\hat{\mathbf{n}}$ to T_i^+ . The quantity $(\mathbf{l_i} \times \hat{\mathbf{n}}) \cdot \mathbf{f_j}(\mathbf{r})$ in eqn. 3.15 is the component of $\mathbf{f_j}$ normal to the i^{th} edge. Since the assumption is made that \mathbf{r} is infinitesimally close to the edge i, this term vanishes but for j=i. Therefore, eqn. 3.15 reduces to

$$[\mathbf{H}^{\text{inc}}(\mathbf{r}_{+}) + \mathbf{H}_{1}^{\text{scat}}(\mathbf{r}_{+})] \cdot \mathbf{l}_{i} = I_{i}^{e}(\mathbf{l}_{i} \times \hat{\mathbf{n}}) \cdot \mathbf{f}_{i}(\mathbf{r})$$
(3.16)

As stated in Sec. 3.2, the '·' product on the right-hand side (RHS) of 3.16 is the component of the vector basis function $\mathbf{f_i}$ normal to the associated edge i, and has

a constant value across the edge. Furthermore, this value is independent of position along $\mathbf{l_i}$. On the other hand, the left-hand side (LHS) of eqn. 3.16 varies along $\mathbf{l_i}$. Nonetheless, the relation can be satisfied in an average sense by integrating both sides of this equation along the common edge i. Therefore, the expansion coefficients I_i^e of the intermediate equivalent electric current can be expressed as

$$I_{\mathbf{i}}^{\mathbf{e}} = \frac{1}{l_{\mathbf{i}}} \int_{\mathbf{l_n}} \left[\mathbf{H}^{\text{inc}}(\mathbf{r}_+) + \mathbf{H}_{\mathbf{1}}^{\text{scat}}(\mathbf{r}_+) \right] \cdot \mathbf{l_i} \ dl$$

$$= \frac{1}{l_{\mathbf{i}}} \int_{\mathbf{l_n}} \mathbf{H}_{\mathbf{1}}^{\text{scat}}(\mathbf{r}_+) \cdot \mathbf{l_i} \ dl + h_{0, \mathbf{i}}$$
(3.17)

where $h_{0, i}$ is due to the incident electric field.

Similarly, the the expansion coefficients $I_{\mathbf{i}}^{\mathbf{e}}$ of the intermediate equivalent magnetic current are given by

$$I_{i}^{m} = -\frac{1}{l_{i}} \int_{l_{n}} \left[\mathbf{E}^{inc}(\mathbf{r}_{+}) + \mathbf{E}_{1}^{scat}(\mathbf{r}_{+}) \right] \cdot \mathbf{l}_{i} \ dl$$

$$= -\frac{1}{l_{i}} \int_{l_{n}} \mathbf{E}_{1}^{scat}(\mathbf{r}_{+}) \cdot \mathbf{l}_{i} \ dl - e_{0, i}$$
(3.18)

where $e_{0,i}$ is due to the incident magnetic filed.

3.4 Construction of the Moment-Method Matrix

In order to solve the problem using the method of moments, one needs to choose the proper testing functions and evaluate the inner product of the field with the testing functions. An advisable testing procedure is to choose the unit vector \mathbf{l}_i and the inner product with a given integrodifferential operator $\mathcal{L}\{\mathbf{f}_i\}$ is defined to satisfy

$$\langle \mathbf{l}_{\mathbf{i}}, \mathcal{L}\{\mathbf{f}_{\mathbf{j}}\} \rangle = \frac{1}{l_{\mathbf{i}}} \int_{\mathbf{l}_{\mathbf{n}}} \mathbf{l}_{\mathbf{i}} \cdot \mathcal{L}\{\mathbf{f}_{\mathbf{j}}\} dl$$
 (3.19)

With the given inner product, the intermediate expansion coefficients $I_{\rm i}^{\rm e}$ and $I_{\rm i}^{\rm m}$

are computed from the coefficients of the effective current $I_{i}^{\mathbf{eff}}$

$$\begin{bmatrix} I^{\mathbf{e}} \\ I^{\mathbf{h}} \end{bmatrix} = \begin{bmatrix} ZW^{\mathbf{e}} \\ ZW^{\mathbf{h}} \end{bmatrix} \begin{bmatrix} I^{\mathbf{eff}} \end{bmatrix}$$
 (3.20)

where $[I^{\mathbf{e}}]$, $[I^{\mathbf{m}}]$ and $[I^{\mathbf{eff}}]$ are length-N column vectors of the respective coefficients, and $[ZW^{\mathbf{e}}]$ and $[ZW^{\mathbf{h}}]$ are $N \times N$ matrices, the entries of which are determined by the pre-defined integral operators in eqn. 2.4 and eqs. 3.17 and 3.18

$$ZW_{ij}^{\mathbf{e}} = \alpha_{i}/2\pi\delta_{ij} - (1 - \delta_{ij})1/l_{i} \int_{\mathbf{l}_{i}} \int_{\mathbf{T}_{j}} \mathbf{l}_{i} \cdot [\mathbf{f}_{j}(\mathbf{r}') \times \nabla G_{1}(\mathbf{r} - \mathbf{r}')]dS' dl$$

$$ZW_{ij}^{\mathbf{m}} = -\frac{j\Omega\mu_{1}}{l_{i}} \int_{\mathbf{l}_{i}} \int_{\mathbf{T}_{j}} \mathbf{l}_{i} \cdot \mathbf{f}_{j}(\mathbf{r}')G_{1}(\mathbf{r} - \mathbf{r}') dS' dl$$

$$-j/l_{i}\Omega\varepsilon_{1} \int_{\mathbf{T}_{j}} \nabla' \cdot \mathbf{f}_{j}(\mathbf{r}')[G_{1}(\mathbf{r}_{i}\mathbf{a} - \mathbf{r}') - G_{1}(\mathbf{r}_{i}^{\mathbf{b}} - \mathbf{r}')] dS'$$

$$(3.21)$$

where $\alpha_{\bf i}$ is the angle between the planes of the triangles $T_{\bf i}^+$ and $T_{\bf i}^-$ measured in the exterior region, $T_{\bf j} = T_{\bf j}^+ + T_{\bf j}^-$ and $\delta_{\bf ij}$ is the Kroneck delta function. Also, ${\bf r}_{\bf i}^{\bf a}$ and ${\bf r}_{\bf i}^{\bf b}$ are the two endpoints of the edge i, such that the unit vector ${\bf l}_{\bf i}$ points from ${\bf r}_{\bf i}^{\bf b}$ to ${\bf r}_{\bf i}^{\bf a}$. $G_1({\bf r}-{\bf r}')$ is the Green's function for the exterior region

$$G_1(\mathbf{r} - \mathbf{r}') = e^{-jk_1}|\mathbf{r} - \mathbf{r}'|/4\pi|\mathbf{r} - \mathbf{r}'|$$
(3.22)

where k_1 is the wavevector in the exterior region.

Applying the same procedure to the MFIE equation 2.21, one can construct the moment-method matrix equation

$$\begin{bmatrix} ZU^{\mathbf{e}} & ZU^{\mathbf{m}} \end{bmatrix} \begin{bmatrix} ZW^{\mathbf{e}} \\ ZW^{\mathbf{h}} \end{bmatrix} \begin{bmatrix} I^{\mathbf{eff}} \end{bmatrix} - [ZW^{\mathbf{e}}] \begin{bmatrix} I^{\mathbf{eff}} \end{bmatrix} = [h_0] + [ZU^{\mathbf{e}}][h_0]$$

$$- [ZU^{\mathbf{m}}][e_0]$$
(3.23)

In the above equation, h_0 and e_0 are the length-N excitation vectors, the elements of which are obtained as

$$h_{0, i} = \int_{\mathbf{l_i}} \mathbf{H}^{inc}(\mathbf{r}) \cdot \mathbf{l_i} dl$$

$$e_{0, i} = \int_{\mathbf{l_i}} \mathbf{E}^{inc}(\mathbf{r}) \cdot \mathbf{l_i} dl$$
(3.24)

 ZU^{e} and ZU^{m} are $N \times N$ matrices, with the entries

$$\begin{split} ZU_{ij}^{\mathbf{e}} &= -\alpha_{i}/2\pi\delta_{ij} + (1-\delta_{ij})1/l_{i} \int_{\mathbf{l}_{i}} \int_{\mathbf{T}_{j}} \mathbf{l}_{i} \cdot [\mathbf{f}_{j}(\mathbf{r}') \times \nabla G_{2}(\mathbf{r} - \mathbf{r}')] dS' \ dl \\ ZU_{ij}^{\mathbf{m}} &= -j\Omega\varepsilon_{1}/l_{i} \int_{\mathbf{l}_{i}} \int_{\mathbf{T}_{j}} \mathbf{l}_{i} \cdot \mathbf{f}_{j}(\mathbf{r}')G_{2}(\mathbf{r} - \mathbf{r}') \ dS' \ dl \\ &- \frac{j}{l_{i}\Omega\mu_{1}} \int_{\mathbf{T}_{j}} \nabla' \cdot \mathbf{f}_{j}(\mathbf{r}')[G_{2}(\mathbf{r}_{i}^{\mathbf{a}} - \mathbf{r}') - G_{1}(\mathbf{r}_{i}^{\mathbf{b}} - \mathbf{r}')] \ dS' \end{split}$$
(3.25)

3.5 Augmenting with the Fast Multipole Method

It is well known that the computational costs and the memory of classical MOM solvers that are augmented by FMM schemes scale as $\mathcal{O}(N_8\log N_8)$ and $\mathcal{O}(N_8)$, respectively. As such, the development of FMM based schemes has been a subject of intense study for a over a decade following the seminal paper by Rokhlin [10]. FMM employs a divide and conquer strategy to reduce the overall computational cost; this is achieved by embedding the body in a fictitious cubical box, and recursively dividing this into eight smaller boxes. A box that is subdivided into smaller boxes is termed the "parent" of the "child" boxes that result from the operation. This leads to a uniform oct-tree structure. For an N+1-level scheme, this subdivision proceeds N times. At the lowest level, the boxes are populated by basis functions or equivalently a set of point electric and magnetic dipoles. Fields due to these dipoles are computed at other locations by upward and downward traversal of the tree. In order to accomplish this in a hierarchical manner, the following dictum is used to create interaction lists:

a pair of boxes at any level are said to be in the far field of each other if the distance between their centers is greater than a prescribed distance and if their parents are in the near field of each other. In practice, this distance, at any level, is chosen to be twice the linear dimension of the box at that level. Thus for any given box at a level greater than one, interactions with boxes in the near field have to be resolved at lower levels in the tree. Interaction with a box in its far field can be computed at a higher level in the tree provided that the respective parent boxes are in the far field of each other.

The matrix equation 3.23 can be solved using the iterative methods, e.g., the transpose-free quasi-minimal residuals method (TFQMR) [11]. TFQMR is accelerated by the FMM method to achieve optimized computation time and memory cost [12].

3.6 Numerical Results

The aim of this section is to test the efficiency and accuracy of the single integral equations discussed in the last section. This is accomplished by applying SIE to the problems of electromagnetic scattering of a plane wave by arbitrary shaped dielectric objects. In what follows, it is assumed that the dielectric scatterer is immersed in the free space ($\varepsilon_1 = \varepsilon_0$, $\mu_1 = \mu_0$, $c_1 = 3 \times 10^8$ m/s), and the material is non-magnetic ($\mu_2 = \mu_0$). These results are compared against the analytical data obtained by the Mie series [13] or the existing computer code based on the Müller formulation.

As shown in Figure 3.4, the scattering from a dielectric sphere of 1 m radius and $\varepsilon_2 = 4\varepsilon_0$, centered at the origin and illuminated by an incident plane wave with $\hat{E}_{\rm X} = \hat{x}$ polarization, $\hat{k} = -\hat{z}$ incident direction, and $f_0 = 250 {\rm MHz}$, is analyzed. There are totally 3600 unknowns involved in solving this problem. The data agree very well with those obtained using the Mie series. However, for this example, the SIE code converges almost twice as fast as that are based on the Müller formulation.

In a second example, scattering from the same sphere as given in Figure 3.4, discretized in terms of 4020 spatial basis functions, is analyzed at $f_0 = 160$ MHz. The sphere is excited by an electromagnetic wave that is $\hat{E}_{\mathbf{X}} = \hat{x}$ polarized and incident from the $\hat{k} = -\hat{z}$ direction. The RCS pattern in the x-y plane compare very well with the Mie series, as illustrated in Figure 3.5.

The next example shows the scattering from a dielectric sphere of the same size but with $\varepsilon_2 = 4\varepsilon_0$. The incident wave is $\hat{E}_{\rm X} = \hat{x}$ polarized, and impinges on the scatterer from the $\hat{k} = -\hat{z}$ direction. The incidence frequency is $f_0 = 225 {\rm MHz}$. There are totally 9414 unknown basis functions. Figure 3.6 demonstrates good agreement between the RCS patterns obtained using the SIE solver and the Müller code.

Our final example of the sphere, given by the second example but analyzed at a higher frequency, is shown in Figure 3.7. The boundary is modeled by 30318 unknown. The incident plane wave at the frequency $f_0 = 300MHz$ is $\hat{E}_{\mathbf{x}} = \hat{x}$ polarized, and illuminates the sphere from the $\hat{k} = -\hat{z}$ direction. Again, results obtained using both SIE equation and Mie series compare satisfactorily.

It turns out that the SIE code can handle not only the smooth geometries, e.g., the sphere, but non-smooth boundaries as well. As shown in Figure 3.8, a cubic box of dimensions 1.0 m×1.0 m×1.0 m is excited by an electromagnetic wave that is polarized in the \hat{x} direction and incident from the $-\hat{z}$ direction. The total number of unknowns is 4077, and the incidence frequency is $f_0 = 257 \text{MHz}$. The agreement between the results obtained by SIE and Müller codes is again very good.

In the last example, scattering from a "fat" almond, discretized using 2208 basis functions is analyzed using SIE and results verified by the Müller formulation, as demonstrated in Figure 3.9. The almond fits in a box of dimensions 1.5 m×1.0 m×0.8 m. The incident field travels in the $\hat{k}=-\hat{z}$ direction, is $\hat{E}_{\rm x}=\hat{x}$ polarized, and has a frequency of $f_0=100{\rm MHz}$.

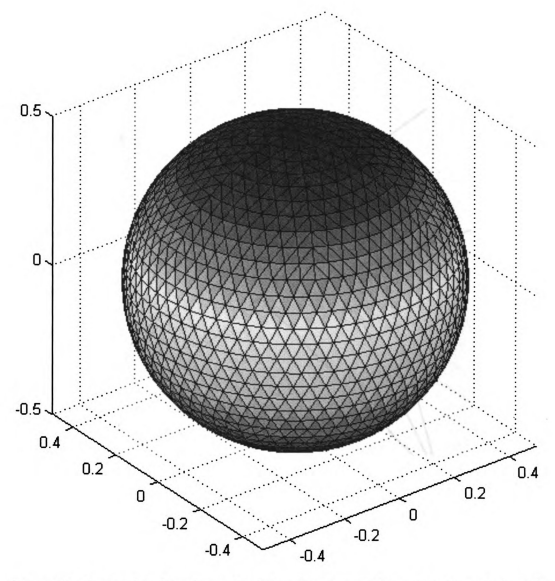


Figure 3.1. Triangulated meshing of a dielectric sphere with r=1.0. The number of triangles is 2904, and the number of edges is 4356.

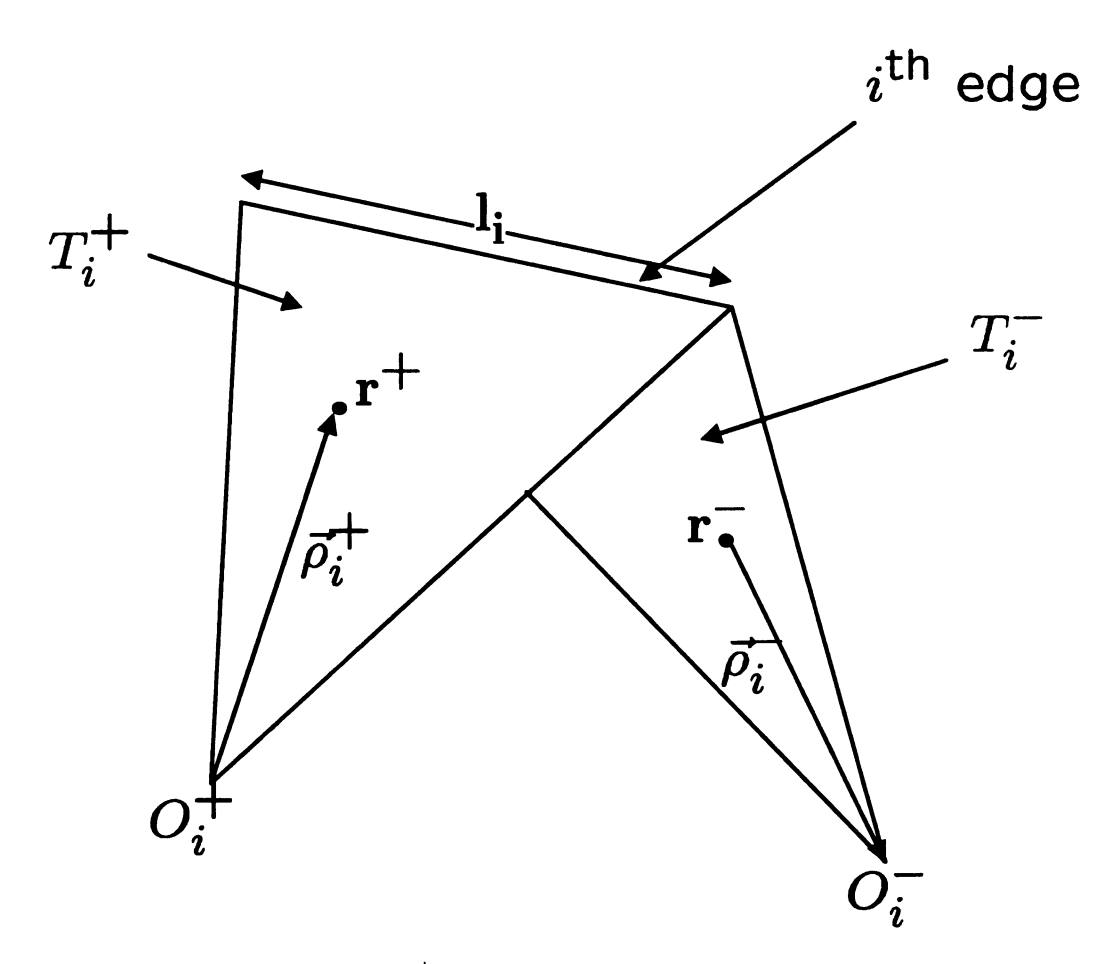


Figure 3.2. Triangle pair (T_i^+, T_i^-) and parameters associated with the ith edge.

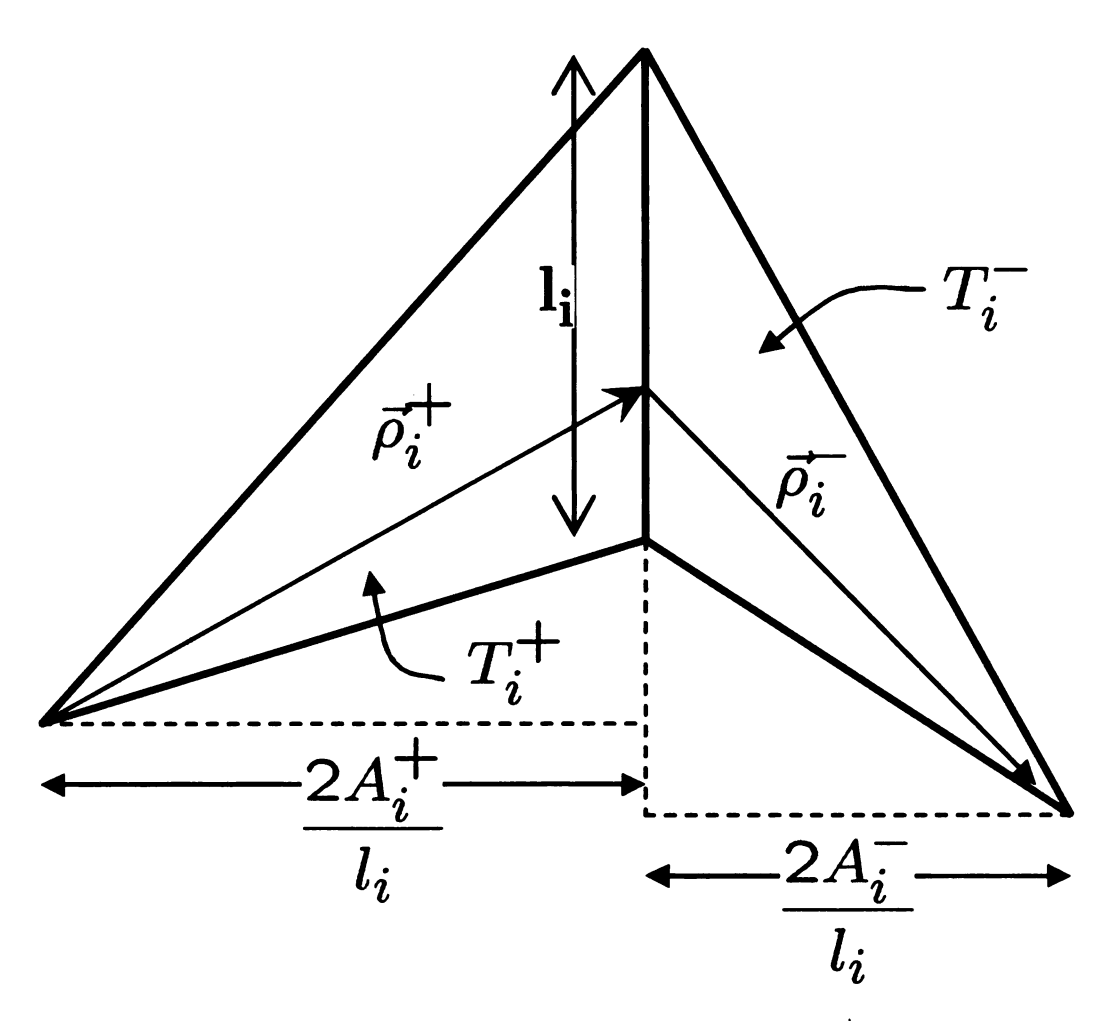


Figure 3.3. Geometry parameters of the triangle pair $T_{\rm i}^+$ and $T_{\rm i}^-$.

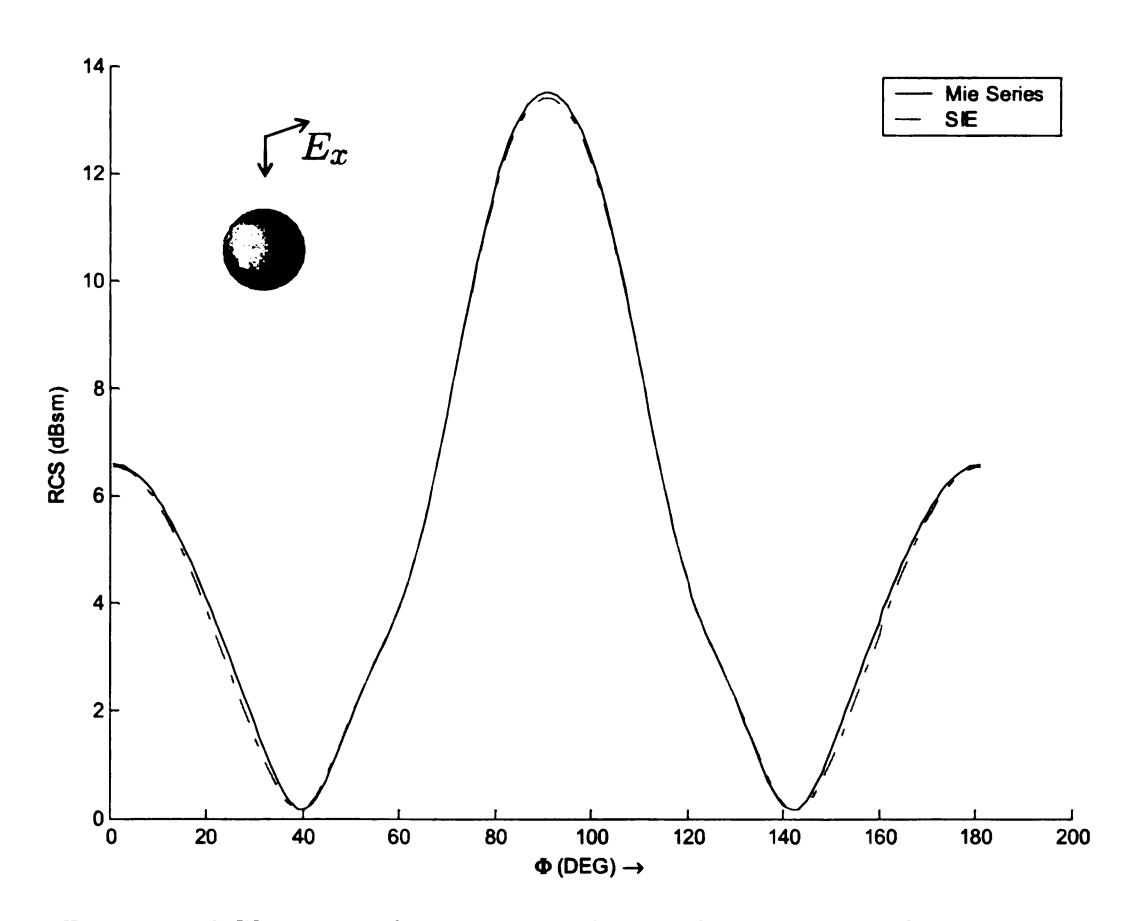


Figure 3.4. RCS pattern of an $\varepsilon_2=2\varepsilon_0$ sphere in the x-y plane at $f_0=160 \mathrm{MHz}$.

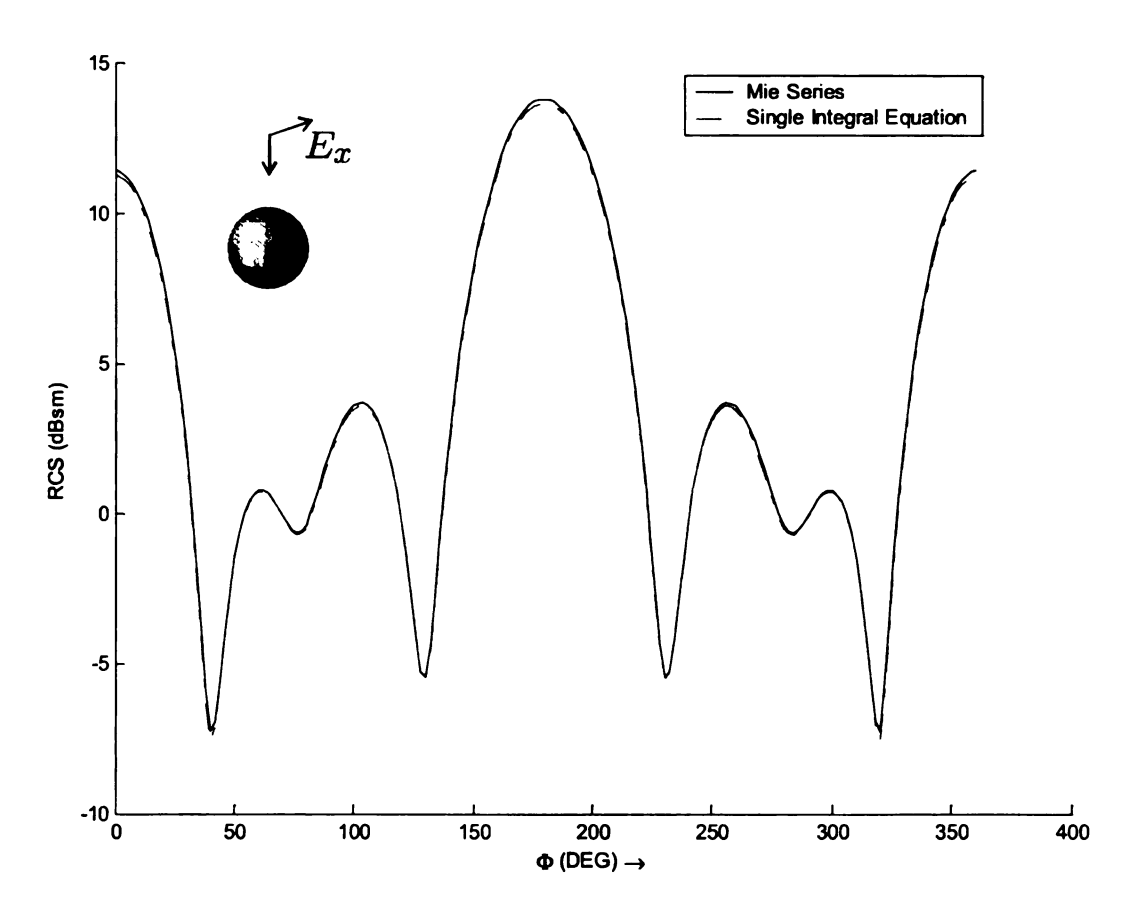


Figure 3.5. RCS pattern of an $\varepsilon_2=4\varepsilon_0$ sphere in the x-y plane at $f_0=160 \mathrm{MHz}.$

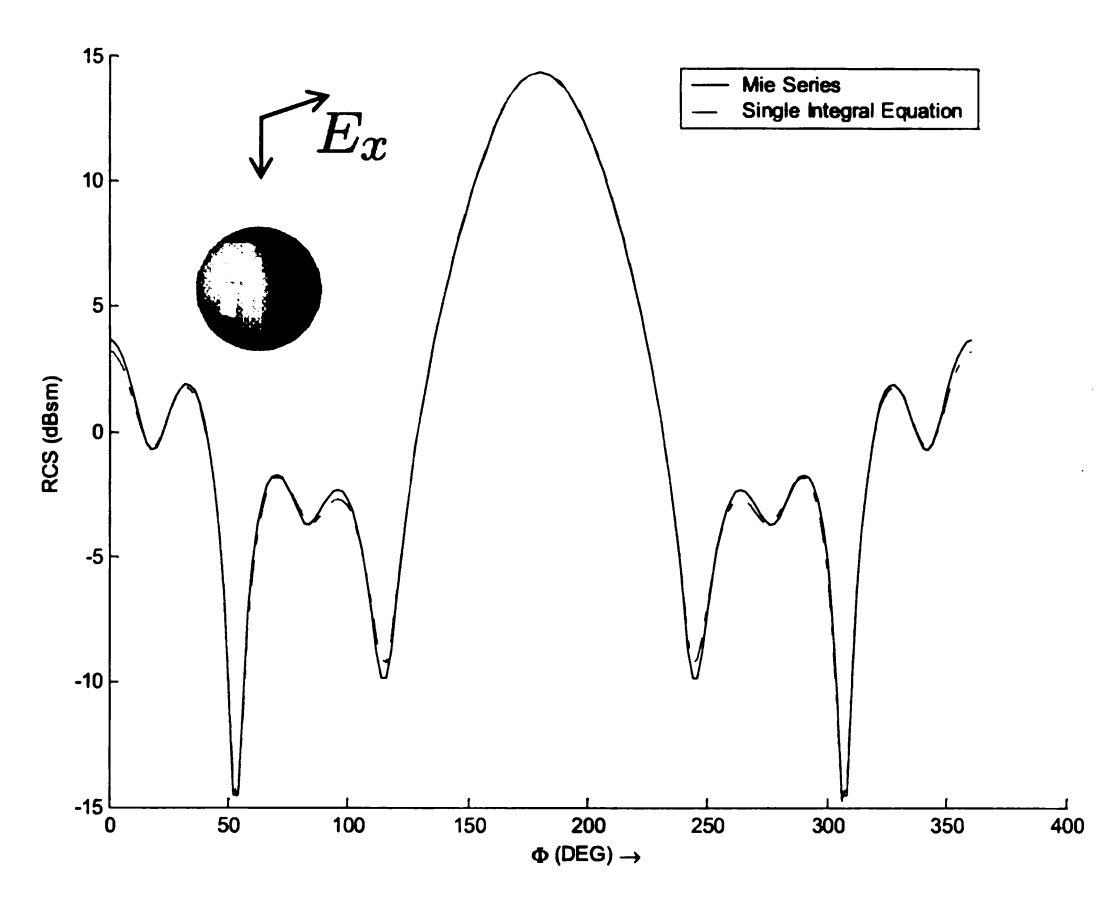


Figure 3.6. RCS pattern of an $\varepsilon_2=4\varepsilon_0$ sphere in the x-y plane at $f_0=225 \mathrm{MHz}.$

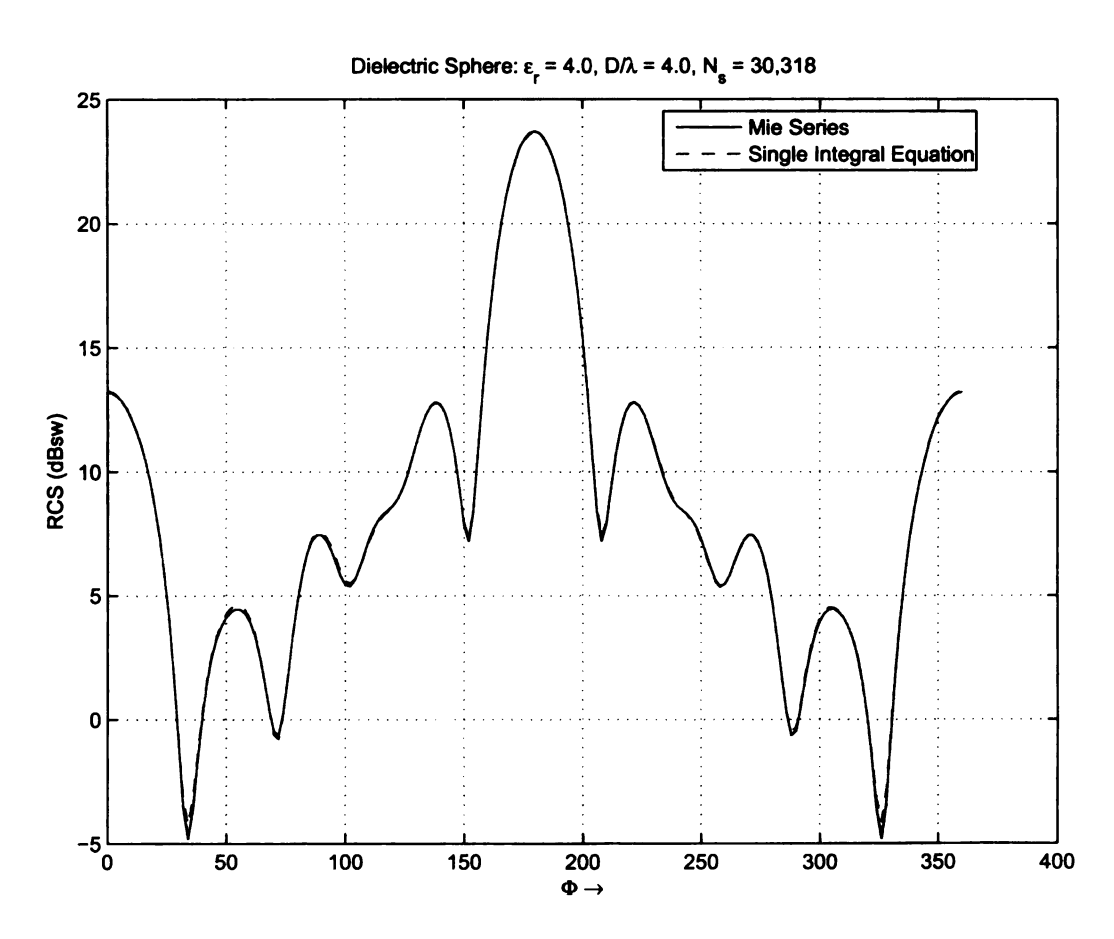


Figure 3.7. RCS pattern of an $\varepsilon_2=4\varepsilon_0$ sphere in the x-y plane at $f_0=300\mathrm{MHz}$.

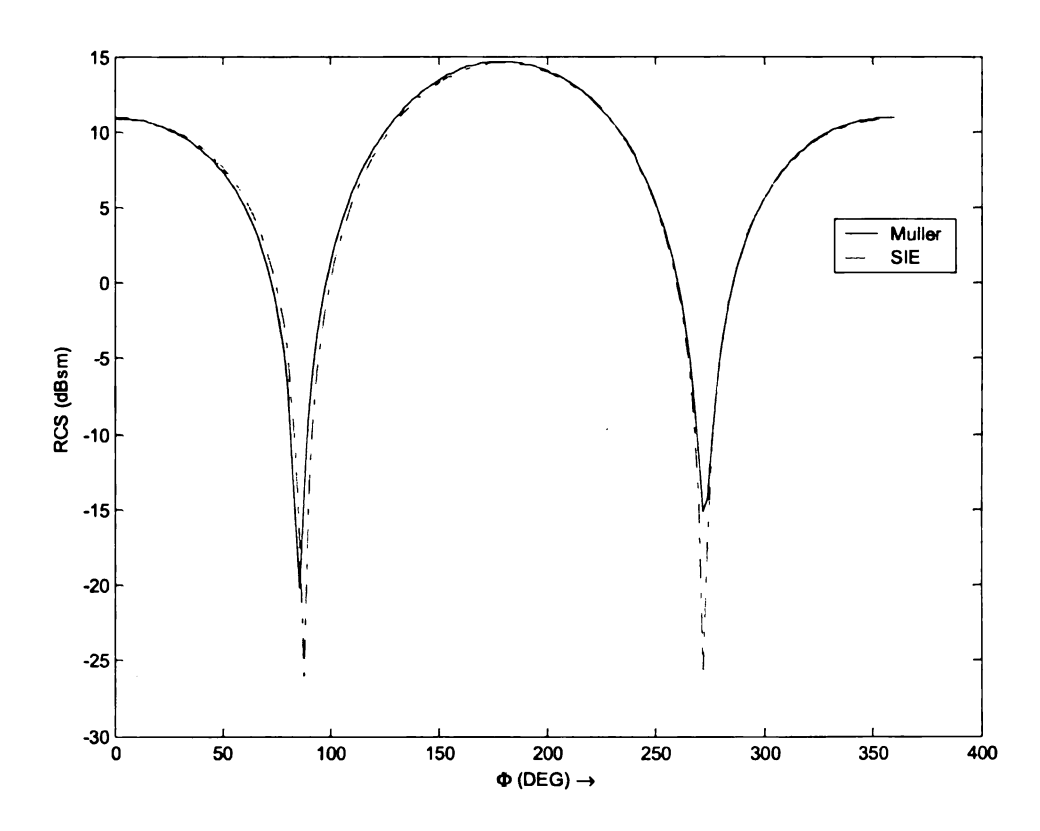


Figure 3.8. RCS pattern of an $\varepsilon_2=4\varepsilon_0$ cubic box in the x-y plane at $f_0=257 \mathrm{MHz}.$

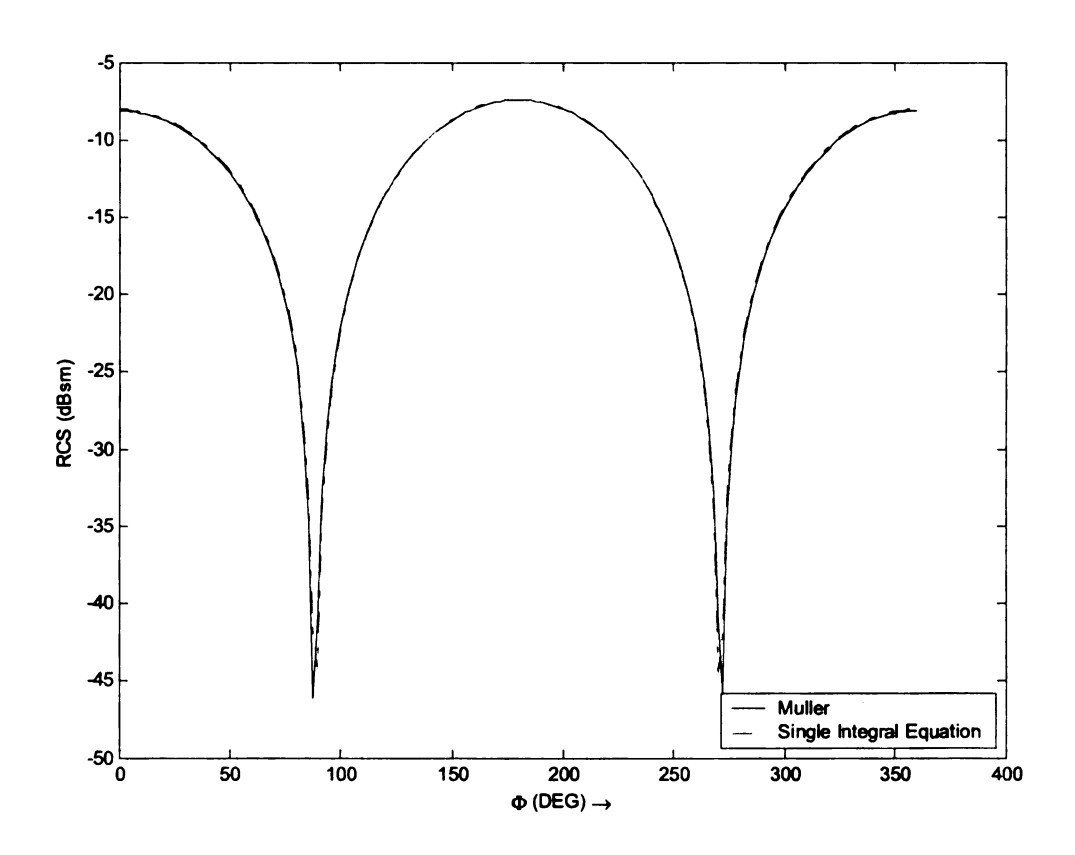


Figure 3.9. RCS pattern of a fat almond in the x-y plane at $f_0 = 100 \mathrm{MHz}$.

CHAPTER 4

SPECTRAL ANALYSIS OF THE SIE OPERATOR

Method for scattering analysis from dielectric objects have been dominated by the PMCHWT and Müller formulations have dominated the computational electromagnetic (CEM) society for decades. However, the constraints as discussed in section 2.2 have prompted the CEM researchers to search for desirable integral formulations. Recent progress in the construction of "fast" methods for the solution of the boundary integral equations, in both frequency [10] and time [14] domains, has vastly expanded the scope of tractable problems.

Most of the integral formulations for analyzing scattering from dielectric bodies to date are in essence various combinations of $L_1\{\star\}$ and $K_1\{\star\}$ operators as given in 2.4. Understanding the performance and behavior of new boundary integral formulations requires a rigorous mathematical investigation of the basic integral operators. Throughout this chapter, we investigate in detail the spectral properties of different operators, and specifically analyze the SIE operator.

4.1 Definition of the Spectrum Analysis

We illustrate spectral analysis of operators used for analyzing scattering from a perfectly conducting (PEC) sphere of radius a. First, any surface current \mathbf{J} on a sphere may be given in terms of the surface Helmholtz decomposition

$$\mathbf{J} = \nabla^{\mathbf{t}} \varphi + \hat{\mathbf{r}} \times \nabla^{\mathbf{t}} \psi \tag{4.1}$$

with

$$\varphi = \sum_{n=1}^{\infty} \sum_{m=-n}^{n} d_{nm}^{1/2} b_{nm} Y_{n}^{m}$$
 (4.2a)

$$\psi = \sum_{n=1}^{\infty} \sum_{m=-n}^{n} d_{nm}^{1/2} c_{nm} Y_{n}^{m}$$
 (4.2b)

where

$$Y_{\mathbf{n}}^{\mathbf{m}}(\hat{\mathbf{r}}) = P_{\mathbf{n}}^{|\mathbf{m}|}(\cos \theta)e^{-\mathbf{j}\mathbf{m}\phi}, \quad n \ge 0, |m| \le n$$

$$(4.3)$$

is the spherical harmonics [1], and

$$d_{\text{nm}} = \frac{(n - |\mathbf{m}|)!(2n + 1)}{(n + |\mathbf{m}|)!4\pi n(n + 1)}$$
(4.4)

is the normalization constant to simplify the subsequent calculations. The coefficients $b_{\rm nm}$ and $c_{\rm nm}$ may be any complex numbers. Using the conjugate relation $\overline{Y}_{\rm n}^{\rm m}=Y_{\rm n}^{\rm -m}$, it is a straightforward exercise to establish the orthogonality of the spherical harmonics:

$$\int_{S} d_{\text{nm}}^{1/2} d_{\text{n'm'}}^{1/2} Y_{\text{n}}^{\text{m}}(\hat{\mathbf{r}}) \overline{Y}_{\text{n'}}^{\text{m'}}(\hat{\mathbf{r}}) dS'
= a^{2} \int_{0}^{2\pi} \int_{0}^{\pi} d_{\text{nm}}^{1/2} d_{\text{n'm'}}^{1/2} P_{\text{n}}^{|\text{m}|}(\cos \theta) P_{\text{n'}}^{|\text{m'}|}(\cos \theta)
e^{-j(\text{m-m'})\phi} \sin \theta d\theta d\phi
= a^{2} \frac{\delta_{\text{nn'}} \delta_{\text{mm'}}}{n(n+1)}$$
(4.5)

$$\int_{S} d_{\text{nm}}^{1/2} d_{\text{n'm'}}^{1/2} \nabla^{t} Y_{\text{n}}^{\text{m}}(\hat{\mathbf{r}}) \cdot \nabla^{t} \overline{Y}_{\text{n'}}^{\text{m'}}(\hat{\mathbf{r}}) dS'$$

$$= \int_{S} d_{\text{nm}}^{1/2} d_{\text{n'm'}}^{1/2} \left[\hat{\mathbf{r}} \times \nabla^{t} Y_{\text{n}}^{\text{m}}(\hat{\mathbf{r}}) \right] \cdot \left[\hat{\mathbf{r}} \times \nabla^{t} \overline{Y}_{\text{n'}}^{\text{m'}}(\hat{\mathbf{r}}) \right] dS'$$

$$= \int_{0}^{2\pi} \int_{0}^{\pi} d_{\text{nm}}^{1/2} d_{\text{n'm'}}^{1/2} \left[\frac{d}{d\theta} P_{\text{n}}^{|\text{m}|}(\cos \theta) \frac{d}{d\theta} P_{\text{n'}}^{|\text{m'}|}(\cos \theta) + \frac{mm'}{\sin^{2} \theta} P_{\text{n}}^{|\text{m}|}(\cos \theta) P_{\text{n'}}^{|\text{m'}|}(\cos \theta) \right] e^{-j(\text{m-m'})\phi} \sin \theta d\theta d\phi$$

$$= \delta_{\text{nn'}} \delta_{\text{mm'}}$$

$$= \delta_{\text{nn'}} \delta_{\text{mm'}}$$
(4.6)

and

$$\int_{S} \nabla^{t} Y_{\mathbf{n}}^{\mathbf{m}}(\hat{\mathbf{r}}) \cdot \left[\hat{\mathbf{r}} \times \nabla^{t} \overline{Y}_{\mathbf{n}'}^{\mathbf{m}'}(\hat{\mathbf{r}}) \right] dS' = 0.$$
(4.7)

In eqs. 4.3 to 4.7, (θ, ϕ) are the spherical polar angles, and $\hat{\mathbf{r}}$ is unit vector normal to the spherical surface. From the equations above, a complete set of basis functions on the surface of a sphere of radius a is given by the vector spherical harmonics

$$\vec{\mathbf{X}}_{nm}(\theta,\phi) = \frac{a}{-j\sqrt{n(n+1)}}\hat{\mathbf{r}} \times \nabla^{t} Y_{n}^{m}(\theta,\phi)$$
 (4.8a)

$$\overrightarrow{\mathbf{U}}_{nm}(\theta,\phi) = \mathbf{\hat{r}} \times \overrightarrow{\mathbf{X}}_{nm}(\theta,\phi) \tag{4.8b}$$

Next, the conventional electric field integral equation (EFIE) and magnetic field integral equation (MFIE) for electromagnetic scattering from PEC surfaces may be rewritten as

$$\hat{\mathbf{n}} \times \mathbf{E}^{\mathrm{inc}} = \eta_1 T_1 \circ \mathbf{J} \tag{4.9}$$

$$\hat{\mathbf{n}} \times \mathbf{H}^{\mathrm{inc}} = \left(\frac{1}{2} + K_1\right) \circ \mathbf{J} \tag{4.10}$$

where the integral operators T_1 and K_1 are defined [15] by

$$T_{1} \circ \mathbf{J} = T(k_{1}) \circ \mathbf{J}$$

$$= -jk_{1} \, \hat{\mathbf{n}} \times \int_{S'} ds' \left\{ G(k_{1}, \mathbf{r}, \mathbf{r}') \mathbf{J}(\mathbf{r}') + \frac{1}{k_{1}^{2}} \nabla \left[\nabla G(k_{1}, \mathbf{r}, \mathbf{r}') \cdot \mathbf{J}(\mathbf{r}') \right] \right\}$$

$$(4.11)$$

$$K_{1} \circ \mathbf{J} = K(k_{1}) \circ \mathbf{J}$$

$$= -\hat{\mathbf{n}} \times \int_{S'} ds' \nabla G(k_{1}, \mathbf{r}, \mathbf{r}') \times \mathbf{J}(\mathbf{r}')$$
(4.12)

Applying T_1 , $K_1^+ \equiv (K_1 + \frac{1}{2})$ and $K_1^- \equiv (K_1 - \frac{1}{2})$ to each basis function in 4.8 yields

$$T(k_1) \circ \left\{ \begin{array}{c} \overrightarrow{\mathbf{X}}_{\mathbf{nm}} \\ \overrightarrow{\mathbf{U}}_{\mathbf{nm}} \end{array} \right\} = \left\{ \begin{array}{c} -\mathbb{J}_{\mathbf{n}}(k_1 a) \mathbb{H}_{\mathbf{n}}(k_1 a) \overrightarrow{\mathbf{U}}_{\mathbf{nm}} \\ \mathbb{J}'_{\mathbf{n}}(k_1 a) \mathbb{H}'_{\mathbf{n}}(k_1 a) \overrightarrow{\mathbf{X}}_{\mathbf{nm}} \end{array} \right\}$$
(4.13)

$$K^{+}(k_{1}) \circ \left\{ \begin{array}{c} \overrightarrow{\mathbf{X}}_{\mathrm{nm}} \\ \overrightarrow{\mathbf{U}}_{\mathrm{nm}} \end{array} \right\} = \left\{ \begin{array}{c} -j \mathbb{J}'_{\mathrm{n}}(k_{1}a) \mathbb{H}_{\mathrm{n}}(k_{1}a) \overrightarrow{\mathbf{X}}_{\mathrm{nm}} \\ j \mathbb{J}_{\mathrm{n}}(k_{1}a) \mathbb{H}'_{\mathrm{n}}(k_{1}a) \overrightarrow{\mathbf{U}}_{\mathrm{nm}} \end{array} \right\}$$
(4.14)

$$K^{-}(k_{1}) \circ \left\{ \begin{array}{c} \overrightarrow{\mathbf{X}}_{nm} \\ \overrightarrow{\mathbf{U}}_{nm} \end{array} \right\} = \left\{ \begin{array}{c} -j \mathbb{J}_{n}(k_{1}a) \mathbb{H}'_{n}(k_{1}a) \overrightarrow{\mathbf{X}}_{nm} \\ j \mathbb{J}'_{n}(k_{1}a) \mathbb{H}_{n}(k_{1}a) \overrightarrow{\mathbf{U}}_{nm} \end{array} \right\}$$
(4.15)

where \mathbb{J}_n and \mathbb{H}_n are Riccati-Bessel and first-kind Riccati-Hankel functions of order n, and k_1 is the wavenumber associated with the kernel of the each integral operator. The Riccati-Bessel and Riccati-Hankel functions are defined in terms of spherical Bessel $j_n(x)$ and Hankel $h_n^{(1)}(x)$ functions by

$$\mathbb{J}_{\mathbf{n}}(x) = xj_{\mathbf{n}}(x) \tag{4.16a}$$

$$\mathbb{H}_{\mathbf{n}}(x) = x h_{\mathbf{n}}^{(1)}(x)$$
 (4.16b)

The spectrum of an integral operator is defined as the function preceding each

basis function on the right-hand-sides in eqs. 4.13, 4.15 and 4.14. There are generally two spectrum factors associated with each basis function, respectively. For the convenience of what follows, $\lambda_{\mathrm{T, \ X}}^{\mathrm{n}}$ denotes the spectrum function of order n due to T operating on $\overrightarrow{\mathbf{X}}$, and $\lambda_{\mathrm{T, \ U}}^{\mathrm{n}}$ represents its $\overrightarrow{\mathbf{U}}$ cousin.

4.2 Spectrum Properties of the Integral Operators

Well-behaved integral operators are the sum of a constant operator and a compact operator (see Appendix). The operators lead to second-kind integral equations, which can be solved with fully controlled error. However, boundary integral operators involved in scattering analysis typically violate this requirement in one or more of three ways.

- 1. The operator may accumulate at zero. A typical example is the spectrum function $\lambda_{\mathrm{T, X}}^{\mathrm{n}}$. As shown in Figure 4.1, a plot of three spectrum curves as a function of k_1a is presented for orders 1, 3 and 5. It is worth noting that for a given k_1a , $\lambda_{\mathrm{T, X}}^{\mathrm{n}}$ eventually vanish, as indicated by the position of point A on the complex plane.
- 2. The operator may have an unbounded spectrum, such as a hypersingular operator. The spectrum function $\lambda_{T, U}^n$ falls into this category. A similar plot in Figure 4.2 demonstrate the singularity of $\lambda_{T, U}^n$ when the order increases. For a fixed $k_1 a$, $\lambda_{T, U}^n$ would eventually blow up to ∞ .
- 3. The operator may have trivial spectrum values associated with resonances, often nonphysical. These are often referred to as "spurious resonances", which can be observed in the case of the operator T_1 .

It is well-known that the MFIE operator (or K_1^+) is a second-kind integral operator. As illustrated in Figure 4.3 and Figure 4.4, both $\lambda_{K^+,X}^n$ and $\lambda_{K^+,U}^n$ converge

to -1/2 in the limit of large n. Therefore, the operator K^+ maintains a bounded spectrum. However, as is evident from eqn. 4.14, Figure 4.3 and Figure 4.4, the operator K^+ yields null eigenvalues at the zeros of $\mathbb{J}'_{\mathbf{n}}(k_1a)$ for $\overrightarrow{\mathbf{X}}_{\mathbf{nm}}$, and at the zeros of $\mathbb{J}_{\mathbf{n}}(k_1a)$ for $\overrightarrow{\mathbf{U}}_{\mathbf{nm}}$, it is not regarded as a well-behaved operator. By the same token, the operator K^- seems spectrally bounded, but is not free of resonances. Similar plots are given in Figure 4.5 and Figure 4.6.

Our analysis shows that the operator T_1 does not have a bounded spectrum, either. Yet a cascaded operator $T^2(k_1) = T(k_1) \circ T(k_1)$ seems to possess better spectral properties.

$$T^{2}(k_{1}) \circ \left\{ \begin{array}{c} \overrightarrow{\mathbf{X}}_{\mathrm{nm}} \\ \overrightarrow{\mathbf{U}}_{\mathrm{nm}} \end{array} \right\} = T_{1}^{2} \circ \left\{ \begin{array}{c} \overrightarrow{\mathbf{X}}_{\mathrm{nm}} \\ \overrightarrow{\mathbf{U}}_{\mathrm{nm}} \end{array} \right\}$$

$$= -\mathbb{J}_{\mathrm{n}}(k_{1}a)\mathbb{H}_{\mathrm{n}}(k_{1}a)\mathbb{J}_{\mathrm{n}}'(k_{1}a)\mathbb{H}_{\mathrm{n}}'(k_{1}a) \left\{ \begin{array}{c} \overrightarrow{\mathbf{X}}_{\mathrm{nm}} \\ \overrightarrow{\mathbf{U}}_{\mathrm{nm}} \end{array} \right\}$$

$$(4.17)$$

It is worth noting that the basis functions $\overrightarrow{\mathbf{X}}_{nm}$ and $\overrightarrow{\mathbf{U}}_{nm}$ are eigenfunctions of the operator $T^2(k_1)$, and its eigenvalues accumulate at -1/4, a result which follows from the asymptotic properties of $j_n(x)$ and $h_n^{(1)}(x)$ [16], and is illustrated in Figure 4.7. An interesting and yet useful derivation [15]

$$K^{+}(k_{1}) \circ K^{-}(k_{1}) \circ \left\{ \begin{array}{c} \overrightarrow{\mathbf{X}}_{nm} \\ \overrightarrow{\mathbf{U}}_{nm} \end{array} \right\}$$

$$= K_{1}^{+} \circ K_{1}^{-} \circ \left\{ \begin{array}{c} \overrightarrow{\mathbf{X}}_{nm} \\ \overrightarrow{\mathbf{U}}_{nm} \end{array} \right\}$$

$$= -\mathbb{J}_{n}(k_{1}a)\mathbb{H}_{n}(k_{1}a)\mathbb{J}'_{n}(k_{1}a)\mathbb{H}'_{n}(k_{1}a) \left\{ \begin{array}{c} \overrightarrow{\mathbf{X}}_{nm} \\ \overrightarrow{\mathbf{U}}_{nm} \end{array} \right\}$$

$$(4.18)$$

reveals the identity

$$T^{2}(k) = K^{2}(k) - \frac{1}{4} = K^{+}(k) \circ K^{-}(k)$$
(4.19)

4.3 Analysis of the SIE Spectrum

Following the notation of the operators T and K, we can rewrite the SIE operator on the left-hand-side of eqn. 2.21 as

$$\mathbf{S_m} \circ \mathbf{J}_{\text{eff}} = \left[K^{-}(k_2) \circ K^{-}(k_1) - \frac{\eta_1}{\eta_2} T(k_2) \circ T(k_1) \right] \circ \mathbf{J}_{\text{eff}}$$
(4.20)

Our previous analysis reveals that both of the operators $T \circ T$ and $K^+ \circ K^-$ have bounded eigenvalues that asymptotically converge, for large order n, to given values. Thus we "predict" that the linear combination of $K_2^- \circ K_1^-$ and $T_2 \circ T_1$ possesses a similar spectral behavior.

It is a straightforward exercise now to derive the eigenvalues of the S_m operator.

$$\begin{split} \mathbf{S_m} \circ \left\{ \begin{array}{l} \overrightarrow{\mathbf{X}}_{\mathrm{nm}} \\ \overrightarrow{\mathbf{U}}_{\mathrm{nm}} \end{array} \right\} &= K^{\text{-}}(k_2) \circ \left\{ \begin{array}{l} -j \mathbb{J}_{\mathrm{n}}(k_1 a) \mathbb{H}'_{\mathrm{n}}(k_1 a) \overrightarrow{\mathbf{X}}_{\mathrm{nm}} \\ j \mathbb{J}'_{\mathrm{n}}(k_1 a) \mathbb{H}_{\mathrm{n}}(k_1 a) \overrightarrow{\mathbf{U}}_{\mathrm{nm}} \end{array} \right\} \\ &- \frac{\eta_1}{\eta_2} T(k_2) \circ \left\{ \begin{array}{l} -\mathbb{J}_{\mathrm{n}}(k_1 a) \mathbb{H}_{\mathrm{n}}(k_1 a) \overrightarrow{\mathbf{U}}_{\mathrm{nm}} \\ \mathbb{J}'_{\mathrm{n}}(k_1 a) \mathbb{H}'_{\mathrm{n}}(k_1 a) \overrightarrow{\mathbf{X}}_{\mathrm{nm}} \end{array} \right\} \\ &= \left\{ \begin{array}{l} -\mathbb{J}_{\mathrm{n}}(k_1 a) \mathbb{H}'_{\mathrm{n}}(k_1 a) \mathbb{J}_{\mathrm{n}}(k_2 a) \mathbb{H}'_{\mathrm{n}}(k_2 a) \overrightarrow{\mathbf{X}}_{\mathrm{nm}} \\ -\mathbb{J}'_{\mathrm{n}}(k_1 a) \mathbb{H}_{\mathrm{n}}(k_1 a) \mathbb{J}'_{\mathrm{n}}(k_2 a) \mathbb{H}_{\mathrm{n}}(k_2 a) \overrightarrow{\mathbf{U}}_{\mathrm{nm}} \end{array} \right\} \\ &- \frac{\eta_1}{\eta_2} \left\{ \begin{array}{l} -\mathbb{J}_{\mathrm{n}}(k_1 a) \mathbb{H}_{\mathrm{n}}(k_1 a) \mathbb{J}'_{\mathrm{n}}(k_2 a) \mathbb{H}'_{\mathrm{n}}(k_2 a) \overrightarrow{\mathbf{X}}_{\mathrm{nm}} \\ -\mathbb{J}'_{\mathrm{n}}(k_1 a) \mathbb{H}'_{\mathrm{n}}(k_1 a) \mathbb{J}_{\mathrm{n}}(k_2 a) \mathbb{H}_{\mathrm{n}}(k_2 a) \overrightarrow{\mathbf{U}}_{\mathrm{nm}} \end{array} \right\} \end{split}$$

$$= \left\{ \begin{array}{l} \mathbb{J}_{\mathbf{n}}(k_{1}a)\mathbb{H}'_{\mathbf{n}}(k_{2}a) \left[\frac{\eta_{1}}{\eta_{2}} \mathbb{J}'_{\mathbf{n}}(k_{2}a)\mathbb{H}_{\mathbf{n}}(k_{1}a) - \mathbb{J}_{\mathbf{n}}(k_{2}a)\mathbb{H}'_{\mathbf{n}}(k_{1}a) \right] \overrightarrow{\mathbf{X}}_{\mathbf{nm}} \\ \mathbb{J}'_{\mathbf{n}}(k_{1}a)\mathbb{H}_{\mathbf{n}}(k_{2}a) \left[\frac{\eta_{1}}{\eta_{2}} \mathbb{J}_{\mathbf{n}}(k_{2}a)\mathbb{H}'_{\mathbf{n}}(k_{1}a) - \mathbb{J}'_{\mathbf{n}}(k_{2}a)\mathbb{H}_{\mathbf{n}}(k_{1}a) \right] \overrightarrow{\mathbf{U}}_{\mathbf{nm}} \end{array} \right\}$$
(4.21)

Figure 4.8 and Figure 4.9 show the eigenvalue curves of a dielectric sphere with $k_2 = 2k_1$. As the order n increases, the eigenvalues accumulate, for the given material contrast ratio, at 1/2 for $\lambda_{\mathbf{Sm},\mathbf{X}}^{\mathbf{n}}$, and at 5/4 for $\lambda_{\mathbf{Sm},\mathbf{U}}^{\mathbf{n}}$. However, the SIE operator $\mathbf{S_m}$ suffers from the internal resonances, due to the fact that the eigenvalues vanish at the zeros of $\mathbb{J}_n(k_1a)$ for the $\overrightarrow{\mathbf{X}}_{nm}$ and at the zeros of $\mathbb{J}'_n(k_1a)$ for the $\overrightarrow{\mathbf{U}}_{nm}$. As a result, the operator $\mathbf{S_m}$ is not regarded as a well-behaved second-kind integral operator, and therefore the SIE formulation, by itself, is not a suitable integral equation for analyzing closed dielectric objects.

Yeung [6] claims that although the EFIE 2.19 and MFIE 2.21 are individually singular at the same resonant frequency, a linear combination of the EFIE and MFIE, namely the CFIE = $[(1 - \alpha)\Delta]$ MFIE + $\alpha\sqrt{\varepsilon_1/\eta_1}$ EFIE, where $0 < \alpha < 1.0$ and Δ is the average length of the triangular-patch model, is non-singular at all frequencies. The operator S_e as in eqn. 2.19 can be expressed in terms of T and K as

$$\mathbf{S}_{e} \circ \mathbf{J}_{eff} = \eta_{1} \left[\frac{\eta_{2}}{\eta_{1}} \hat{\mathbf{r}} \times T(k_{2}) \circ K^{-}(k_{1}) + \hat{\mathbf{r}} \times K^{-}(k_{2}) \circ T(k_{1}) \right] \circ \mathbf{J}_{eff}$$
(4.22)

And the eigenvalues can be obtained

$$\begin{split} \mathbf{S_e} & \circ \left\{ \begin{array}{l} \overrightarrow{\mathbf{X}}_{\mathrm{nm}} \\ \overrightarrow{\mathbf{U}}_{\mathrm{nm}} \end{array} \right\} \\ & = \eta_1 \left[\frac{\eta_2}{\eta_1} \hat{\mathbf{r}} \times T(k_2) \circ \left\{ \begin{array}{l} -j \mathbb{J}_{\mathrm{n}}(k_1 a) \mathbb{H}'_{\mathrm{n}}(k_1 a) \overrightarrow{\mathbf{X}}_{\mathrm{nm}} \\ j \mathbb{J}'_{\mathrm{n}}(k_1 a) \mathbb{H}_{\mathrm{n}}(k_1 a) \overrightarrow{\mathbf{U}}_{\mathrm{nm}} \end{array} \right\} \\ & + \hat{\mathbf{r}} \times K^{-}(k_2) \circ \left\{ \begin{array}{l} -\mathbb{J}_{\mathrm{n}}(k_1 a) \mathbb{H}_{\mathrm{n}}(k_1 a) \overrightarrow{\mathbf{U}}_{\mathrm{nm}} \\ \mathbb{J}'_{\mathrm{n}}(k_1 a) \mathbb{H}'_{\mathrm{n}}(k_1 a) \overrightarrow{\mathbf{X}}_{\mathrm{nm}} \end{array} \right\} \right] \end{split}$$

$$= \eta_{1} \left[\frac{\eta_{2}}{\eta_{1}} \hat{\mathbf{r}} \times \left\{ \begin{array}{l} j \mathbb{J}_{n}(k_{1}a) \mathbb{H}'_{n}(k_{1}a) \mathbb{J}_{n}(k_{2}a) \mathbb{H}_{n}(k_{2}a) \overrightarrow{\mathbf{U}}_{nm} \\ \mathbb{J}'_{n}(k_{1}a) \mathbb{H}_{n}(k_{1}a) \mathbb{J}'_{n}(k_{2}a) \mathbb{H}'_{n}(k_{2}a) \overrightarrow{\mathbf{X}}_{nm} \end{array} \right\}$$

$$+ \hat{\mathbf{r}} \times \left\{ \begin{array}{l} -j \mathbb{J}_{n}(k_{1}a) \mathbb{H}_{n}(k_{1}a) \mathbb{J}'_{n}(k_{2}a) \mathbb{H}_{n}(k_{2}a) \overrightarrow{\mathbf{U}}_{nm} \\ -j \mathbb{J}'_{n}(k_{1}a) \mathbb{H}'_{n}(k_{1}a) \mathbb{J}_{n}(k_{2}a) \mathbb{H}'_{n}(k_{2}a) \overrightarrow{\mathbf{X}}_{nm} \end{array} \right\}$$

$$= \eta_{1} \left[\frac{\eta_{2}}{\eta_{1}} \left\{ \begin{array}{l} -j \mathbb{J}_{n}(k_{1}a) \mathbb{H}'_{n}(k_{1}a) \mathbb{J}_{n}(k_{2}a) \mathbb{H}'_{n}(k_{2}a) \overrightarrow{\mathbf{X}}_{nm} \\ \mathbb{J}'_{n}(k_{1}a) \mathbb{H}_{n}(k_{1}a) \mathbb{J}'_{n}(k_{2}a) \mathbb{H}'_{n}(k_{2}a) \overrightarrow{\mathbf{U}}_{nm} \end{array} \right\}$$

$$+ \left\{ \begin{array}{l} j \mathbb{J}_{n}(k_{1}a) \mathbb{H}_{n}(k_{1}a) \mathbb{J}'_{n}(k_{2}a) \mathbb{H}_{n}(k_{2}a) \overrightarrow{\mathbf{X}}_{nm} \\ -j \mathbb{J}'_{n}(k_{1}a) \mathbb{H}'_{n}(k_{1}a) \mathbb{J}_{n}(k_{2}a) \mathbb{H}'_{n}(k_{2}a) \overrightarrow{\mathbf{U}}_{nm} \end{array} \right\}$$

$$= \eta_{1} \left\{ \begin{array}{l} j \mathbb{J}_{n}(k_{1}a) \mathbb{H}_{n}(k_{2}a) \left[\mathbb{J}'_{n}(k_{2}a) \mathbb{H}_{n}(k_{1}a) \\ -\frac{\eta_{2}}{\eta_{1}} \mathbb{J}'_{n}(k_{2}a) \mathbb{H}'_{n}(k_{1}a) \right] \overrightarrow{\mathbf{X}}_{nm} \\ -j \mathbb{J}'_{n}(k_{1}a) \mathbb{H}'_{n}(k_{2}a) \left[\mathbb{J}_{n}(k_{2}a) \mathbb{H}'_{n}(k_{1}a) \\ -\frac{\eta_{2}}{\eta_{1}} \mathbb{J}'_{n}(k_{2}a) \mathbb{H}_{n}(k_{1}a) \right] \overrightarrow{\mathbf{U}}_{nm} \end{array} \right\}$$

However, as is evident from eqs. 4.3 and 4.23, the operator $\mathbf{S_e}$ shares resonances (at the zeros of $\mathbb{J}_n(k_1a)$ for the $\overrightarrow{\mathbf{X}}_{nm}$ modes, and at the zeros of $\mathbb{J}'_n(k_1a)$ for the $\overrightarrow{\mathbf{U}}_{nm}$ modes) with the SIE operator $\mathbf{S_m}$. This is a disproof of the conclusions drawn by Yeung [6].

4.4 Well-behaved CSIE Operator

One possible remedy for the spurious resonance is the addition of an equivalent magnetic current \mathbf{M}_{eff} on Ω^+ , with the constraint [17] that

$$\mathbf{M}_{\mathbf{eff}} = \eta_1 \hat{\mathbf{r}} \times \mathbf{J}_{\mathbf{eff}} \tag{4.24}$$

This additional current would give rise to an new term on the left-hand-side of the SIE equation, denoted as

$$\mathbf{S_{m}}^{\dagger} \circ \mathbf{M_{eff}} = -\left[K^{-}(k_2) \circ T(k_1) + \frac{\eta_1}{\eta_2} T(k_2) \circ K^{-}(k_1)\right] \circ \mathbf{M_{eff}}$$
(4.25)

And by operating on the spherical harmonic, the eigenvalues for $\mathbf{S_m}^{\dagger}$ are obtained

$$S_{\mathbf{m}^{\dagger}} \circ \left\{ \eta_{1} \hat{\mathbf{r}} \times \begin{bmatrix} \overrightarrow{\mathbf{X}}_{nm} \\ \overrightarrow{\mathbf{U}}_{nm} \end{bmatrix} \right\}$$

$$= -\eta_{1} \left[K^{-}(k_{2}) \circ T(k_{1}) + \frac{\eta_{1}}{\eta_{2}} T(k_{2}) \circ K^{-}(k_{1}) \right] \circ \left\{ \overrightarrow{\mathbf{U}}_{nm} \right\}$$

$$= \eta_{1} \left[K^{-}(k_{2}) \circ \left\{ J'_{n}(k_{1}a) \mathbb{H}'_{n}(k_{1}a) \overrightarrow{\mathbf{X}}_{nm} \right\} \right\}$$

$$+ \frac{\eta_{1}}{\eta_{2}} T(k_{2}) \circ \left\{ J'_{n}(k_{1}a) \mathbb{H}_{n}(k_{1}a) \overrightarrow{\mathbf{U}}_{nm} \right\}$$

$$+ \frac{\eta_{1}}{\eta_{2}} T(k_{2}) \circ \left\{ J''_{n}(k_{1}a) \mathbb{H}_{n}(k_{1}a) \overrightarrow{\mathbf{U}}_{nm} \right\}$$

$$= \eta_{1} \left\{ -j J'_{n}(k_{1}a) \mathbb{H}'_{n}(k_{1}a) \mathbb{J}_{n}(k_{2}a) \mathbb{H}'_{n}(k_{2}a) \overrightarrow{\mathbf{X}}_{nm} \right\}$$

$$+ \eta_{1} \left\{ -j J'_{n}(k_{1}a) \mathbb{H}_{n}(k_{1}a) J'_{n}(k_{2}a) \mathbb{H}_{n}(k_{2}a) \overrightarrow{\mathbf{U}}_{nm} \right\}$$

$$+ \frac{\eta_{1}}{\eta_{2}} \left\{ -j J'_{n}(k_{1}a) \mathbb{H}_{n}(k_{1}a) J'_{n}(k_{2}a) \mathbb{H}'_{n}(k_{2}a) \overrightarrow{\mathbf{X}}_{nm} \right\}$$

$$-j J_{n}(k_{1}a) \mathbb{H}'_{n}(k_{1}a) J'_{n}(k_{2}a) \mathbb{H}'_{n}(k_{1}a) - \frac{\eta_{1}}{\eta_{2}} J'_{n}(k_{2}a) \mathbb{H}_{n}(k_{1}a) \right\} \overrightarrow{\mathbf{X}}_{nm}$$

$$= \eta_{1} \left\{ -j J'_{n}(k_{1}a) \mathbb{H}'_{n}(k_{2}a) \left[J_{n}(k_{2}a) \mathbb{H}'_{n}(k_{1}a) - \frac{\eta_{1}}{\eta_{2}} J'_{n}(k_{2}a) \mathbb{H}'_{n}(k_{1}a) \right] \overrightarrow{\mathbf{X}}_{nm} \right\}$$

$$= \eta_{1} \left\{ -j J'_{n}(k_{1}a) \mathbb{H}'_{n}(k_{2}a) \left[J'_{n}(k_{2}a) \mathbb{H}'_{n}(k_{1}a) - \frac{\eta_{1}}{\eta_{2}} J'_{n}(k_{2}a) \mathbb{H}'_{n}(k_{1}a) \right] \overrightarrow{\mathbf{U}}_{nm} \right\}$$

$$= \eta_{1} \left\{ -j J'_{n}(k_{1}a) \mathbb{H}'_{n}(k_{2}a) \left[J'_{n}(k_{2}a) \mathbb{H}'_{n}(k_{1}a) - \frac{\eta_{1}}{\eta_{2}} J'_{n}(k_{2}a) \mathbb{H}'_{n}(k_{1}a) \right] \overrightarrow{\mathbf{U}}_{nm} \right\}$$

$$= \eta_{1} \left\{ -j J'_{n}(k_{1}a) \mathbb{H}'_{n}(k_{2}a) \left[J'_{n}(k_{2}a) \mathbb{H}'_{n}(k_{1}a) - \frac{\eta_{1}}{\eta_{2}} J'_{n}(k_{2}a) \mathbb{H}'_{n}(k_{1}a) \right] \overrightarrow{\mathbf{U}}_{nm} \right\}$$

$$= \eta_{1} \left\{ -j J'_{n}(k_{1}a) \mathbb{H}'_{n}(k_{2}a) \left[J'_{n}(k_{2}a) \mathbb{H}'_{n}(k_{1}a) - \frac{\eta_{1}}{\eta_{2}} J'_{n}(k_{2}a) \mathbb{H}'_{n}(k_{1}a) \right] \overrightarrow{\mathbf{U}}_{nm} \right\}$$

Apparently, they don't share any zeros with the eigenvalues of operator S. Thus, we can write an expression for a well-behaved combined source single integral equation

(CSIE) operator

$$\mathbf{S}_{\mathrm{cs}} \circ \mathbf{J}_{\mathrm{eff}} = \mathbf{S}_{\mathbf{m}} \circ \mathbf{J}_{\mathrm{eff}} + \mathbf{S}_{\mathbf{m}}^{\dagger} \circ (\hat{\mathbf{n}} \times \mathbf{J}_{\mathrm{eff}})$$

$$= \left[K^{-}(k_{2}) \circ K^{-}(k_{1}) - \frac{\eta_{1}}{\eta_{2}} T(k_{2}) \circ T(k_{1}) \right] \circ \mathbf{J}_{\mathrm{eff}}$$

$$- \eta_{1} \left[K^{-}(k_{2}) \circ T(k_{1}) + \frac{\eta_{1}}{\eta_{2}} T(k_{2}) \circ K^{-}(k_{1}) \right] \circ (\hat{\mathbf{n}} \times \mathbf{J}_{\mathrm{eff}})$$

$$(4.27)$$

The condition number of the CSIE, though larger than that of the SIE, is still dominated by the well-behaved property of **S**.

4.5 An alternative integral equation scheme

It should be noted that the CSIE formulation is not the only approach for eliminating the spurious resonances. We spend the rest of this chapter analyzing an integral equation scheme from a different perspective.

At interior resonant frequencies, the **E** field tangential to Ω calculated from the SIE surface currents is not continuous across the boundary. It follows that the **H** field normal to Ω will not necessarily be continuous. It is suggested that the inclusion of the normal boundary conditions of the magnetic field would augment the SIE to yield the unique exterior solution at all frequencies [18],[19].

$$\hat{\mathbf{n}} \cdot [\mu_2 \mathbf{H}_2^{\text{scat}}] = \hat{\mathbf{n}} \cdot [\mu_1 (\mathbf{H}^{\text{inc}} + \mathbf{H}_1^{\text{scat}})]$$
(4.28)

It can be re-written, in analog to eqn. 2.17, in the following form.

$$\hat{\mathbf{n}} \cdot [\mu_{1}\mathbf{H}^{\mathrm{inc}}] = \hat{\mathbf{n}} \cdot (\frac{\mu_{2}}{\eta_{2}}\mathbf{L}_{2}\{\mathbf{M}_{2}\} + \mu_{2}\mathbf{K}_{2}\{\mathbf{J}_{2}\} - \mu_{1}\mathbf{K}_{1}\{\mathbf{J}_{\mathrm{eff}}\})$$

$$= \hat{\mathbf{n}} \cdot \left(\frac{\mu_{2}}{\eta_{2}}\mathbf{L}_{2}\{-\mathbf{E}^{\mathrm{inc}} \times \hat{\mathbf{n}} - \eta_{1}\mathbf{L}_{1}\{\mathbf{J}_{\mathrm{eff}}\} \times \hat{\mathbf{n}}\}\right)$$

$$+ \mu_{2}\mathbf{K}_{2}\{-\hat{\mathbf{n}} \times \mathbf{H}^{\mathrm{inc}} - \hat{\mathbf{n}} \times \mathbf{K}_{1}\{\mathbf{J}_{\mathrm{eff}}\}\}$$

$$-\mu_{1}\mathbf{K}_{1}\{\mathbf{J}_{\mathrm{eff}}\})$$

$$= \hat{\mathbf{n}} \cdot \left(\frac{1}{c_{2}}\mathbf{L}_{2}\{-\mathbf{E}^{\mathrm{inc}} \times \hat{\mathbf{n}} - \eta_{1}\mathbf{L}_{1}\{\mathbf{J}_{\mathrm{eff}}\} \times \hat{\mathbf{n}}\}\right)$$

$$+ \mu_{2}\mathbf{K}_{2}\{-\hat{\mathbf{n}} \times \mathbf{H}^{\mathrm{inc}} - \hat{\mathbf{n}} \times \mathbf{K}_{1}\{\mathbf{J}_{\mathrm{eff}}\}\}$$

$$-\mu_{1}\mathbf{K}_{1}\{\mathbf{J}_{\mathrm{eff}}\})$$

where $c_2 = 1/\sqrt{\varepsilon_2\mu_2}$ is the velocity of light in the interior media.

Rearrangement of the terms in the above equation gives the "augmented" single integral equation (ASIE)

$$\hat{\mathbf{n}} \cdot \mu_2 \mathbf{K}_2 \{ \hat{\mathbf{n}} \times \mathbf{K}_1 \{ \mathbf{J}_{\text{eff}} \} \} + \frac{\eta_1}{c_2} \hat{\mathbf{n}} \cdot \mathbf{L}_2 \{ \hat{\mathbf{n}} \times \mathbf{L}_1 \{ \mathbf{J}_{\text{eff}} \} \} - \hat{\mathbf{n}} \cdot \mu_1 \mathbf{K}_1 \{ \mathbf{J}_{\text{eff}} \} = \mathbf{H}_{\text{rhs}}^{\square}$$
 (4.30)

where

$$\mathbf{H}_{\text{rhs}}^{\square} = \hat{\mathbf{n}} \cdot \mu_1 \mathbf{H}^{\text{inc}} + \hat{\mathbf{n}} \cdot \mu_2 \mathbf{K}_2 \{ \hat{\mathbf{n}} \times \mathbf{H}^{\text{inc}} \} - \frac{1}{c_2} \hat{\mathbf{n}} \cdot \mathbf{L}_2 \{ \hat{\mathbf{n}} \times \mathbf{E}^{\text{inc}} \}$$
(4.31)

Next, we prove that this ASIE shares no resonance with the existing SIE spectrum. By inspection, two differences can be observed between ASIE and eqn. 2.20.

- Due to the normal product $(\hat{\mathbf{n}}\cdot)$, ASIE is a scalar equation;
- $\bullet \ \, \text{The term } -\hat{\mathbf{n}}\cdot\mu_1\mathbf{K}_1\{\mathbf{J}_{\text{eff}}\} \text{ cannot be combined with } \hat{\mathbf{n}}\cdot\mu_2\mathbf{K}_2\{\hat{\mathbf{n}}\times\mathbf{K}_1\{\mathbf{J}_{\text{eff}}\}\}.$

Using notation similar to eqn. (4.20), we define the ASIE operator as

$$\mathbf{S}_{\mathbf{m}}^{\mathbf{a}} \circ \mathbf{J}_{\mathbf{eff}} = \left\{ -\mu_{2} \hat{\mathbf{n}} \cdot \left[\mathbf{K}_{2} \circ K(k_{1}) \right] + \frac{\eta_{1}}{c_{2}} \hat{\mathbf{n}} \cdot \left[\mathbf{L}_{2} \circ T(k_{1}) \right] - \mu_{1} \hat{\mathbf{n}} \cdot \mathbf{K}_{1} \right\} \circ \mathbf{J}_{\mathbf{eff}} \quad (4.32)$$

Utilizing the mapping of $T \longleftrightarrow \hat{\mathbf{n}} \times \mathbf{L}$ and $K \longleftrightarrow -\hat{\mathbf{n}} \times \mathbf{K}$, and representing the unknown \mathbf{J}_{eff} with $\overrightarrow{\mathbf{X}}_{\text{nm}}$ and $\overrightarrow{\mathbf{U}}_{\text{nm}}$, the right-hand-side of the ASIE equation can be rewritten as

$$\mathbf{S}_{\mathbf{m}}^{\mathbf{a}} \circ \overrightarrow{\mathbf{X}}_{\mathbf{nm}} = \left\{ -\mu_{2} \hat{\mathbf{n}} \cdot \left[\mathbf{K}_{2} \circ K(k_{1}) \right] + \frac{\eta_{1}}{c_{2}} \hat{\mathbf{n}} \cdot \left[\mathbf{L}_{2} \circ T(k_{1}) \right] - \mu_{1} \hat{\mathbf{n}} \cdot \mathbf{K}_{1} \right\} \circ \overrightarrow{\mathbf{X}}_{\mathbf{nm}}$$

$$= -\mu_{2} \hat{\mathbf{n}} \cdot \mathbf{K}_{2} \circ \left[K(k_{1}) \circ \overrightarrow{\mathbf{X}}_{\mathbf{nm}} \right] + \frac{\eta_{1}}{c_{2}} \hat{\mathbf{n}} \cdot \mathbf{L}_{2} \circ \left[T(k_{1}) \circ \overrightarrow{\mathbf{X}}_{\mathbf{nm}} \right]$$

$$- \mu_{1} \hat{\mathbf{n}} \cdot \left[\mathbf{K}_{1} \circ \overrightarrow{\mathbf{X}}_{\mathbf{nm}} \right]$$

$$= -\mu_{2} \hat{\mathbf{n}} \cdot \mathbf{K}_{2} \circ \left[K^{+}(k_{1}) - \frac{1}{2} \right] \circ \overrightarrow{\mathbf{X}}_{\mathbf{nm}} + \frac{\eta_{1}}{c_{2}} \hat{\mathbf{n}} \cdot \mathbf{L}_{2} \circ \left[T(k_{1}) \circ \overrightarrow{\mathbf{X}}_{\mathbf{nm}} \right]$$

$$- \mu_{1} \hat{\mathbf{n}} \cdot \left[\mathbf{K}_{1} \circ \overrightarrow{\mathbf{X}}_{\mathbf{nm}} \right]$$

$$= -\mu_{2} \hat{\mathbf{n}} \cdot \mathbf{K}_{2} \circ \left[K^{+}(k_{1}) \circ \overrightarrow{\mathbf{X}}_{\mathbf{nm}} \right] + \frac{\eta_{1}}{c_{2}} \hat{\mathbf{n}} \cdot \mathbf{L}_{2} \circ \left[T(k_{1}) \circ \overrightarrow{\mathbf{X}}_{\mathbf{nm}} \right]$$

$$- \mu_{1} \hat{\mathbf{n}} \cdot \left[\mathbf{K}_{1} \circ \overrightarrow{\mathbf{X}}_{\mathbf{nm}} \right] - \frac{1}{2} \mu_{2} \hat{\mathbf{n}} \cdot \left[\mathbf{K}_{2} \circ \overrightarrow{\mathbf{X}}_{\mathbf{nm}} \right]$$

$$= j \mu_{2} \mathbf{J}'_{\mathbf{n}}(k_{1}a) \mathbf{H}_{\mathbf{n}}(k_{1}a) \left\{ \hat{\mathbf{n}} \cdot \left[\mathbf{L}_{2} \circ \overrightarrow{\mathbf{X}}_{\mathbf{nm}} \right] \right\}$$

$$- \mu_{1} \hat{\mathbf{n}} \cdot \left[\mathbf{K}_{1} \circ \overrightarrow{\mathbf{X}}_{\mathbf{nm}} \right] - \frac{1}{2} \mu_{2} \hat{\mathbf{n}} \cdot \left[\mathbf{K}_{2} \circ \overrightarrow{\mathbf{X}}_{\mathbf{nm}} \right]$$

$$= \mu_{2} \left(j \mathbf{J}'_{\mathbf{n}}(k_{1}a) \mathbf{H}_{\mathbf{n}}(k_{1}a) - \frac{1}{2} \right) \left\{ \hat{\mathbf{n}} \cdot \left[\mathbf{K}_{2} \circ \overrightarrow{\mathbf{X}}_{\mathbf{nm}} \right] \right\}$$

$$- \frac{\eta_{1}}{c_{2}} \mathbf{J}_{\mathbf{n}}(k_{1}a) \mathbf{H}_{\mathbf{n}}(k_{1}a) \left\{ \hat{\mathbf{n}} \cdot \left[\mathbf{L}_{2} \circ \overrightarrow{\mathbf{U}}_{\mathbf{nm}} \right] \right\}$$

$$- \mu_{1} \hat{\mathbf{n}} \cdot \left[\mathbf{K}_{1} \circ \overrightarrow{\mathbf{X}}_{\mathbf{nm}} \right]$$

$$- \mu_{1} \hat{\mathbf{n}} \cdot \left[\mathbf{K}_{1} \circ \overrightarrow{\mathbf{X}}_{\mathbf{nm}} \right]$$

$$(4.33)$$

`

and

$$\mathbf{S}_{\mathbf{m}}^{\mathbf{a}} \circ \overrightarrow{\mathbf{U}}_{\mathbf{n}\mathbf{m}} = \left\{ -\mu_{2}\hat{\mathbf{n}} \cdot \left[\mathbf{K}_{2} \circ K(k_{1}) \right] + \frac{\eta_{1}}{c_{2}}\hat{\mathbf{n}} \cdot \left[\mathbf{L}_{2} \circ T(k_{1}) \right] - \mu_{1}\hat{\mathbf{n}} \cdot \mathbf{K}_{1} \right\} \circ \overrightarrow{\mathbf{U}}_{\mathbf{n}\mathbf{m}}$$

$$= -\mu_{2}\hat{\mathbf{n}} \cdot \mathbf{K}_{2} \circ \left[K(k_{1}) \circ \overrightarrow{\mathbf{U}}_{\mathbf{n}\mathbf{m}} \right] + \frac{\eta_{1}}{c_{2}}\hat{\mathbf{n}} \cdot \mathbf{L}_{2} \circ \left[T(k_{1}) \circ \overrightarrow{\mathbf{U}}_{\mathbf{n}\mathbf{m}} \right]$$

$$- \mu_{1}\hat{\mathbf{n}} \cdot \left[\mathbf{K}_{1} \circ \overrightarrow{\mathbf{U}}_{\mathbf{n}\mathbf{m}} \right]$$

$$= -\mu_{2}\hat{\mathbf{n}} \cdot \mathbf{K}_{2} \circ \left[K^{+}(k_{1}) - \frac{1}{2} \right] \circ \overrightarrow{\mathbf{U}}_{\mathbf{n}\mathbf{m}} + \frac{\eta_{1}}{c_{2}}\hat{\mathbf{n}} \cdot \mathbf{L}_{2} \circ \left[T(k_{1}) \circ \overrightarrow{\mathbf{U}}_{\mathbf{n}\mathbf{m}} \right]$$

$$- \mu_{1}\hat{\mathbf{n}} \cdot \left[\mathbf{K}_{1} \circ \overrightarrow{\mathbf{U}}_{\mathbf{n}\mathbf{m}} \right]$$

$$= -\mu_{2}\hat{\mathbf{n}} \cdot \mathbf{K}_{2} \circ \left[K^{+}(k_{1}) \circ \overrightarrow{\mathbf{U}}_{\mathbf{n}\mathbf{m}} \right] + \frac{\eta_{1}}{c_{2}}\hat{\mathbf{n}} \cdot \mathbf{L}_{2} \circ \left[T(k_{1}) \circ \overrightarrow{\mathbf{U}}_{\mathbf{n}\mathbf{m}} \right]$$

$$- \mu_{1}\hat{\mathbf{n}} \cdot \left[\mathbf{K}_{1} \circ \overrightarrow{\mathbf{U}}_{\mathbf{n}\mathbf{m}} \right] - \frac{1}{2}\mu_{2}\hat{\mathbf{n}} \cdot \left[\mathbf{K}_{2} \circ \overrightarrow{\mathbf{U}}_{\mathbf{n}\mathbf{m}} \right]$$

$$= -j\mu_{2}\mathbb{J}_{\mathbf{n}}(k_{1}a)\mathbb{H}'_{\mathbf{n}}(k_{1}a) \left\{ \hat{\mathbf{n}} \cdot \left[\mathbf{K}_{2} \circ \overrightarrow{\mathbf{U}}_{\mathbf{n}\mathbf{m}} \right] \right\}$$

$$+ \frac{\eta_{1}}{c_{2}}\mathbb{J}'_{\mathbf{n}}(k_{1}a)\mathbb{H}'_{\mathbf{n}}(k_{1}a) + \frac{1}{2}\mu_{2}\hat{\mathbf{n}} \cdot \left[\mathbf{K}_{2} \circ \overrightarrow{\mathbf{U}}_{\mathbf{n}\mathbf{m}} \right]$$

$$= -\mu_{2}\left(j\mathbb{J}_{\mathbf{n}}(k_{1}a)\mathbb{H}'_{\mathbf{n}}(k_{1}a) + \frac{1}{2}\right) \left\{ \hat{\mathbf{n}} \cdot \left[\mathbf{K}_{2} \circ \overrightarrow{\mathbf{U}}_{\mathbf{n}\mathbf{m}} \right] \right\}$$

$$+ \frac{\eta_{1}}{c_{2}}\mathbb{J}'_{\mathbf{n}}(k_{1}a)\mathbb{H}'_{\mathbf{n}}(k_{1}a) \left\{ \hat{\mathbf{n}} \cdot \left[\mathbf{L}_{2} \circ \overrightarrow{\mathbf{X}}_{\mathbf{n}\mathbf{m}} \right] \right\}$$

$$- \mu_{1}\hat{\mathbf{n}} \cdot \left[\mathbf{K}_{1} \circ \overrightarrow{\mathbf{U}}_{\mathbf{n}\mathbf{m}} \right]$$

$$- \mu_{1}\hat{\mathbf{n}} \cdot \left[\mathbf{K}_{1} \circ \overrightarrow{\mathbf{U}}_{\mathbf{n}\mathbf{m}} \right]$$

$$(4.34)$$

Denoting

$$\Phi_{\mathrm{nm}}^{x}(k_{1}) = \hat{\mathbf{n}} \cdot [\mathbf{K}_{1} \circ \overrightarrow{\mathbf{X}}_{\mathrm{nm}}]$$
 (4.35a)

$$\Phi_{\text{nm}}^{u}(k_1) = \hat{\mathbf{n}} \cdot [\mathbf{K}_1 \circ \overrightarrow{\mathbf{U}}_{\text{nm}}] \tag{4.35b}$$

$$\Phi_{\text{nm}}^{x}(k_2) = \hat{\mathbf{n}} \cdot [\mathbf{K}_2 \circ \overrightarrow{\mathbf{X}}_{\text{nm}}] \tag{4.35c}$$

$$\Phi_{nm}^{u}(k_2) = \hat{\mathbf{n}} \cdot [\mathbf{K}_2 \circ \overrightarrow{\mathbf{U}}_{nm}] \tag{4.35d}$$

$$\Psi_{\text{nm}}^{x}(k_2) = \hat{\mathbf{n}} \cdot [\mathbf{L}_2 \circ \overrightarrow{\mathbf{X}}_{\text{nm}}] \tag{4.35e}$$

$$\Psi_{\text{nm}}^{u}(k_2) = \hat{\mathbf{n}} \cdot [\mathbf{L}_2 \circ \overrightarrow{\mathbf{U}}_{\text{nm}}] \tag{4.35f}$$

we may present eqs. 4.33 and 4.34 in slightly different forms

$$\mathbf{S_{m}^{a}} \circ \overrightarrow{\mathbf{X}}_{nm} = \mu_{2} \left[j \mathbb{J}'_{n}(k_{1}a) \mathbb{H}_{n}(k_{1}a) - \frac{1}{2} \right] \Phi_{nm}^{x}(k_{2}) - \frac{\eta_{1}}{c_{2}} \mathbb{J}_{n}(k_{1}a) \mathbb{H}_{n}(k_{1}a) \Psi_{nm}^{u}(k_{2}) - \mu_{1} \Phi_{nm}^{x}(k_{1})$$

$$(4.36)$$

$$\mathbf{S_{m}^{a}} \circ \overrightarrow{\mathbf{U}}_{nm} = -\mu_{2} \left[j \mathbb{J}_{n}(k_{1}a) \mathbb{H}'_{n}(k_{1}a) + \frac{1}{2} \right] \Phi_{nm}^{u}(k_{2}) + \frac{\eta_{1}}{c_{2}} \mathbb{J}'_{n}(k_{1}a) \mathbb{H}'_{n}(k_{1}a) \Psi_{nm}^{x}(k_{2}) - \mu_{1} \Phi_{nm}^{u}(k_{1})$$

$$(4.37)$$

In the above eqn. 4.36, it is obvious that the coefficient $\left[j\mathbb{J}'_{\mathbf{n}}(k_{1}a)\mathbb{H}_{\mathbf{n}}(k_{1}a)-\frac{1}{2}\right]$ doesn't share nulls with $\mathbb{J}_{\mathbf{n}}(k_{1}a)\mathbb{H}_{\mathbf{n}}(k_{1}a)$. $\left[j\mathbb{J}'_{\mathbf{n}}(k_{1}a)\mathbb{H}_{\mathbf{n}}(k_{1}a)-\frac{1}{2}\right]$ has only complex roots, while on the contrary, zeros of $\mathbb{J}_{\mathbf{n}}(k_{1}a)\mathbb{H}_{\mathbf{n}}(k_{1}a)$ are all real. Therefore, at least one of these two terms has non-trivial value at the interior resonant frequencies. By the same token, the term $\mathbf{S}^{\mathbf{a}}_{\mathbf{m}} \circ \overrightarrow{\mathbf{U}}_{\mathbf{n}\mathbf{m}}$ yields finite right-hand-side in eqn. 4.37. It is also worth noting that neither $\Phi^{\mathbf{x}/\mathbf{u}}_{\mathbf{n}\mathbf{m}}(k_{2})$ nor $\Psi^{\mathbf{x}/\mathbf{u}}_{\mathbf{n}\mathbf{m}}(k_{2})$ in eqs. 4.36 and 4.37 would support a interior resonance mode. This is because $\Phi^{\mathbf{x}/\mathbf{u}}_{\mathbf{n}\mathbf{m}}(k_{2})$ and $\Psi^{\mathbf{x}/\mathbf{u}}_{\mathbf{n}\mathbf{m}}(k_{2})$ depend solely on k_{2} , and although they may vanish at certain frequencies pertaining to the

interior media (k_2) , it is only at the resonant frequencies associated with the exterior media (k_1) that the SIE operator would fail.

These desirable properties of ASIE make it suitable for augmenting eqn. 4.21,

$$\mathbf{S_{m}} \circ \overrightarrow{\mathbf{X}}_{nm} = \mathbb{J}_{n}(k_{1}a)\mathbb{H}'_{n}(k_{2}a) \left[\frac{\eta_{1}}{\eta_{2}} \mathbb{J}'_{n}(k_{2}a)\mathbb{H}_{n}(k_{1}a) - \mathbb{J}_{n}(k_{2}a)\mathbb{H}'_{n}(k_{1}a) \right] \overrightarrow{\mathbf{X}}_{nm} \quad (4.38)$$

$$\mathbf{S_{m}} \circ \overrightarrow{\mathbf{X}}_{nm} = \mathbb{J}_{n}(k_{1}a)\mathbb{H}'_{n}(k_{2}a) \left[\frac{\eta_{1}}{\eta_{2}} \mathbb{J}'_{n}(k_{2}a)\mathbb{H}_{n}(k_{1}a) - \mathbb{J}_{n}(k_{2}a)\mathbb{H}'_{n}(k_{1}a) \right] \overrightarrow{\mathbf{X}}_{nm} \quad (4.38)$$

$$\mathbf{S_{m}} \circ \overrightarrow{\mathbf{U}}_{nm} = \mathbb{J}'_{n}(k_{1}a)\mathbb{H}_{n}(k_{2}a) \left[\frac{\eta_{1}}{\eta_{2}} \mathbb{J}_{n}(k_{2}a)\mathbb{H}'_{n}(k_{1}a) - \mathbb{J}'_{n}(k_{2}a)\mathbb{H}_{n}(k_{1}a) \right] \overrightarrow{\mathbf{U}}_{nm} \quad (4.39)$$

to circumvent the resonance deficiency of SIE.

$$\begin{cases}
\mathbf{S}_{\mathbf{m}}^{\mathbf{a}} \circ \overrightarrow{\mathbf{X}}_{nm} = \mu_{2} \left[j \mathbb{J}'_{n}(k_{1}a) \mathbb{H}_{n}(k_{1}a) - \frac{1}{2} \right] \Phi_{nm}^{x}(k_{2}) \\
- \frac{\eta_{1}}{c_{2}} \mathbb{J}_{n}(k_{1}a) \mathbb{H}_{n}(k_{1}a) \Psi_{nm}^{u}(k_{2}) - \mu_{1} \Phi_{nm}^{x}(k_{1})
\end{cases}$$

$$\mathbf{S}_{\mathbf{m}} \circ \overrightarrow{\mathbf{X}}_{nm} = \mathbb{J}_{n}(k_{1}a) \mathbb{H}'_{n}(k_{2}a) \left[\frac{\eta_{1}}{\eta_{2}} \mathbb{J}'_{n}(k_{2}a) \mathbb{H}_{n}(k_{1}a) - \mathbb{J}_{n}(k_{2}a) \mathbb{H}'_{n}(k_{1}a) \right] \overrightarrow{\mathbf{X}}_{nm}$$

$$\begin{cases}
\mathbf{S}_{\mathbf{m}}^{\mathbf{a}} \circ \overrightarrow{\mathbf{U}}_{nm} = -\mu_{2} \left[j \mathbb{J}_{n}(k_{1}a) \mathbb{H}'_{n}(k_{1}a) + \frac{1}{2} \right] \Phi_{nm}^{u}(k_{2}) \\
+ \frac{\eta_{1}}{c_{2}} \mathbb{J}'_{n}(k_{1}a) \mathbb{H}'_{n}(k_{1}a) \Psi_{nm}^{x}(k_{2}) - \mu_{1} \Phi_{nm}^{u}(k_{1})
\end{cases}$$

$$\begin{cases}
\mathbf{S}_{\mathbf{m}} \circ \overrightarrow{\mathbf{U}}_{nm} = \mathbb{J}'_{n}(k_{1}a) \mathbb{H}'_{n}(k_{2}a) \left[\frac{\eta_{1}}{\eta_{2}} \mathbb{J}_{n}(k_{2}a) \mathbb{H}'_{n}(k_{1}a) - \mathbb{J}'_{n}(k_{2}a) \mathbb{H}_{n}(k_{1}a) \right] \overrightarrow{\mathbf{U}}_{nm}
\end{cases}$$

$$(4.41)$$

At interior resonant frequencies, i.e., nulls corresponds to $\mathbb{J}_{\mathbf{n}}(k_1a)$ or $\mathbb{J}'_{\mathbf{n}}(k_1a)$, eqs. 4.40 and 4.45 would reduce to

$$\begin{cases}
\mathbf{S_{m}^{a}} \circ \overrightarrow{\mathbf{X}}_{nm} = \mu_{2} \left[j \mathbb{J}'_{n}(k_{1}a) \mathbb{H}_{n}(k_{1}a) - \frac{1}{2} \right] \Phi_{nm}^{x}(k_{2}) - \mu_{1} \Phi_{nm}^{x}(k_{1}) \\
\mathbf{S_{m}} \circ \overrightarrow{\mathbf{X}}_{nm} = \mathbf{0}
\end{cases} (4.42)$$

$$\begin{cases}
\mathbf{S}_{\mathbf{m}}^{\mathbf{a}} \circ \overrightarrow{\mathbf{U}}_{\mathbf{n}\mathbf{m}} = -\frac{1}{2}\mu_{2}\Phi_{\mathbf{n}\mathbf{m}}^{u}(k_{2}) + \frac{\eta_{1}}{c_{2}}\mathbb{J}_{\mathbf{n}}^{\prime}(k_{1}a)\mathbb{H}_{\mathbf{n}}^{\prime}(k_{1}a)\Psi_{\mathbf{n}\mathbf{m}}^{x}(k_{2}) - \mu_{1}\Phi_{\mathbf{n}\mathbf{m}}^{u}(k_{1}) \\
\mathbf{S}_{\mathbf{m}} \circ \overrightarrow{\mathbf{U}}_{\mathbf{n}\mathbf{m}} = \mathbb{J}_{\mathbf{n}}^{\prime}(k_{1}a)\mathbb{H}_{\mathbf{n}}(k_{2}a)\left[\frac{\eta_{1}}{\eta_{2}}\mathbb{J}_{\mathbf{n}}(k_{2}a)\mathbb{H}_{\mathbf{n}}^{\prime}(k_{1}a) - \mathbb{J}_{\mathbf{n}}^{\prime}(k_{2}a)\mathbb{H}_{\mathbf{n}}(k_{1}a)\right]\overrightarrow{\mathbf{U}}_{\mathbf{n}\mathbf{m}} \\
(4.43)
\end{cases}$$

for $\mathbb{J}_{\mathbf{n}}(k_1a) = 0$, respectively, and

$$\begin{cases}
\mathbf{S}_{\mathbf{m}}^{\mathbf{a}} \circ \overrightarrow{\mathbf{X}}_{\mathbf{nm}} = -\frac{\eta_{1}}{c_{2}} \mathbb{J}_{\mathbf{n}}(k_{1}a) \mathbb{H}_{\mathbf{n}}(k_{1}a) \Psi_{\mathbf{nm}}^{u}(k_{2}) - \mu_{1} \Phi_{\mathbf{nm}}^{x}(k_{1}) \\
\mathbf{S}_{\mathbf{m}} \circ \overrightarrow{\mathbf{X}}_{\mathbf{nm}} = \mathbb{J}_{\mathbf{n}}(k_{1}a) \mathbb{H}'_{\mathbf{n}}(k_{2}a) \left[\frac{\eta_{1}}{\eta_{2}} \mathbb{J}'_{\mathbf{n}}(k_{2}a) \mathbb{H}_{\mathbf{n}}(k_{1}a) - \mathbb{J}_{\mathbf{n}}(k_{2}a) \mathbb{H}'_{\mathbf{n}}(k_{1}a) \right] \overrightarrow{\mathbf{X}}_{\mathbf{nm}} \\
\begin{cases}
\mathbf{S}_{\mathbf{m}}^{\mathbf{a}} \circ \overrightarrow{\mathbf{U}}_{\mathbf{nm}} = -\mu_{2} \left[j \mathbb{J}_{\mathbf{n}}(k_{1}a) \mathbb{H}'_{\mathbf{n}}(k_{1}a) + \frac{1}{2} \right] \Phi_{\mathbf{nm}}^{u}(k_{2}) - \mu_{1} \Phi_{\mathbf{nm}}^{u}(k_{1}) \\
\mathbf{S}_{\mathbf{m}} \circ \overrightarrow{\mathbf{U}}_{\mathbf{nm}} = \mathbf{0}
\end{cases} (4.45)$$

for $\mathbb{J}'_{\mathbf{n}}(k_1a) = 0$.

Now, the foregoing analysis should suffice to conclude that by solving SIE and ASIE, together,

$$\mathbf{S_m} \circ \mathbf{J_{eff}} = \mathbf{H_{rhs}} \tag{4.46a}$$

$$\mathbf{S}_{\mathbf{m}}^{\mathbf{a}} \circ \mathbf{J}_{\mathbf{eff}} = \mathbf{H}_{\mathbf{rhs}}^{\square} \tag{4.46b}$$

spurious resonances from the exterior scattering or radiating problem can be eliminated.

4.6 Implementation and solution of the augmented integral equations

From the prior analysis, one can say that ASIE is a viable remedy for the interior resonant issue of SIE. However, it proves no advantage unless several difficulties are addressed when implemented using MoM.

- ullet The augmented equations are overdetermined. Two equations need to be solved for only one unknown current ${f J}_{
 m eff}$
- Cascaded operators, e.g., $K^{\text{-}}(k_2) \circ K^{\text{-}}(k_1)$ and $T(k_2) \circ T(k_1)$, are encountered

in eqs. 4.46, and they can possess hyper-singular component, especially for $T(k_2) \circ T(k_1)$.

• Both vector and scalar equations show up in the augmented equations.

There is a standard procedure for finding the least-squared solution to an overdetermined set of equations [18], [20]. Thus we are allowed to solve eqs. 4.46 by multiplying the equations by the Hermitian conjugate of its coefficient matrix, and then solving the resulting even-determined, Hermitian set of equations. Since we have proved that the overdetermined equations can yield a unique solution at all frequencies, the least-squared solution becomes identical to this unique solution.

As for the second bullet, appropriate intermediate projection spaces need to be chosen discretely for the each of the inner products. Adams $et\ al.[21]$ have proposed using the surface Helmholtz complement of the RWG subspace $(\{\hat{\mathbf{n}}\times\mathbf{f}_i\}_{i=1}^N)$ for the intermediate projection. With the appropriate projection subspaces, a correct discretization procedure for the $T(k_2)\circ T(k_1)$ operator can be achieved.

Since eqn. 4.46b is a scalar function, a set of scalar testing functions are required. Pisharody et al. [19] recently reported that spatial scalar testing functions can be constructed using the Silvester polynomials [22] in the normalized parametric coordinates. The most straight-forward category are the "hat" functions, which are unity at a given node, vanish at all neighboring nodes.

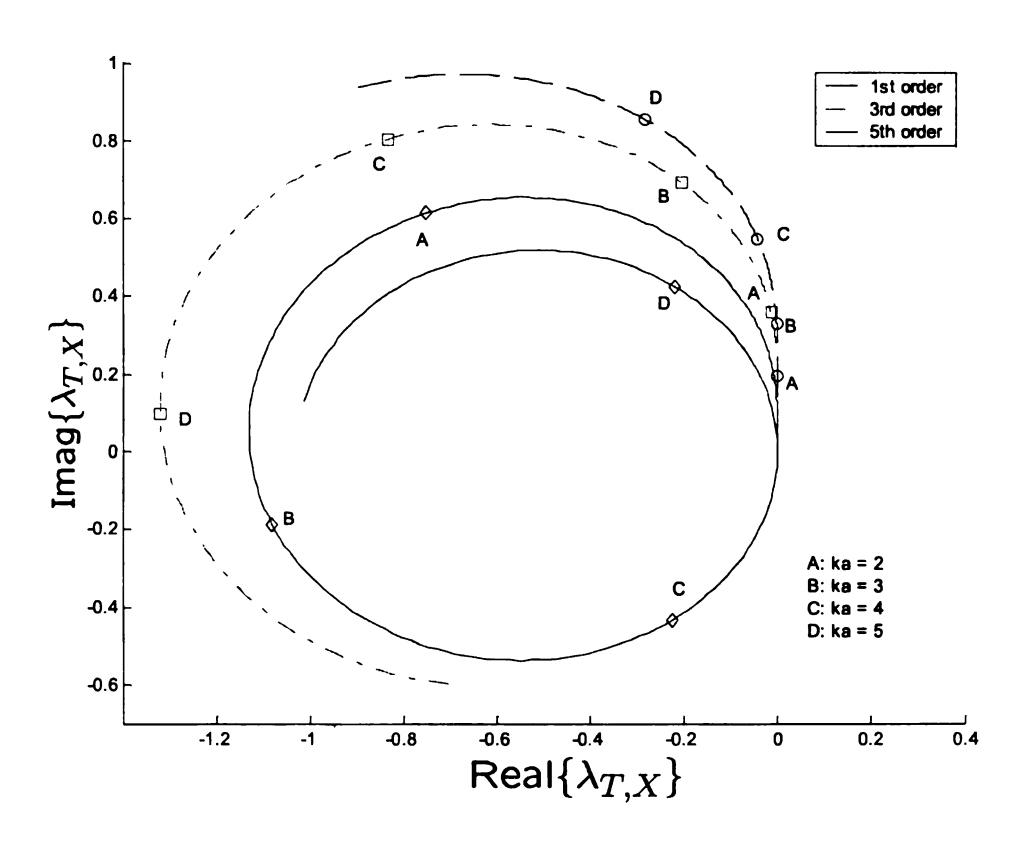


Figure 4.1. Plot of three spectral functions of $\lambda_{\mathrm{T,\ X}}^{\mathrm{n}}$ for $k_1a\in[0.01,6],$ and $n\in[1,3,5].$

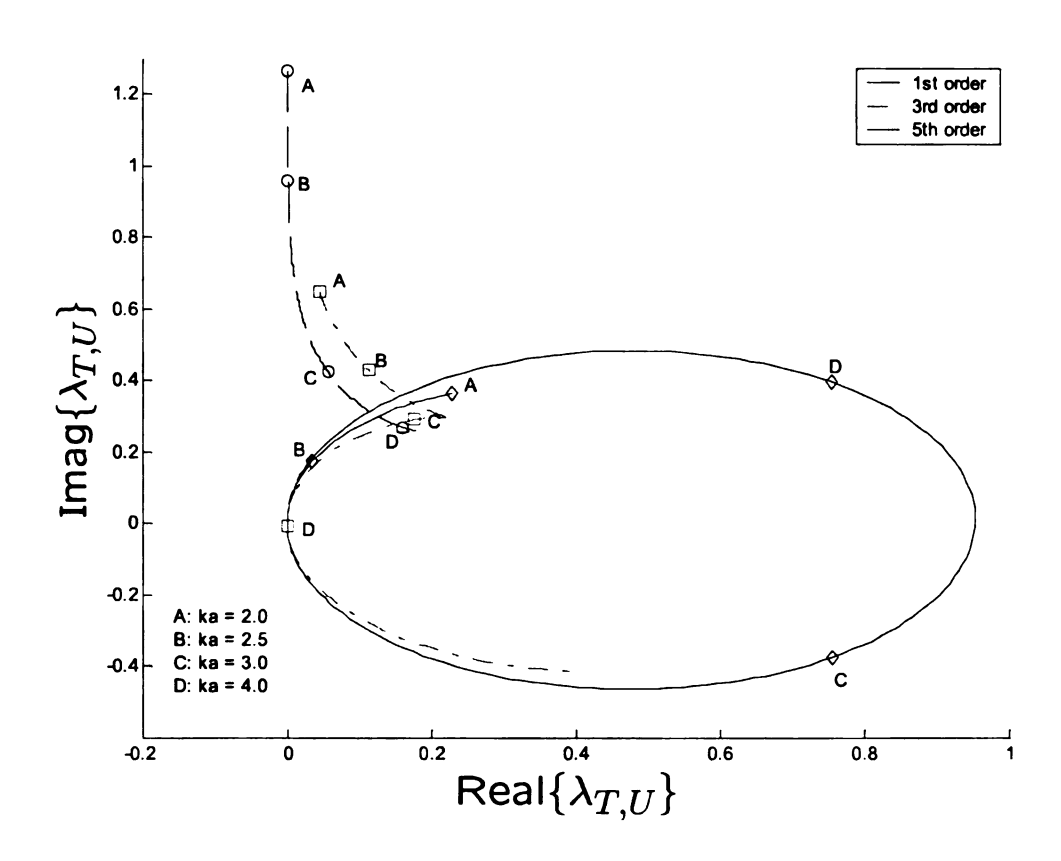


Figure 4.2. Plot of three spectral functions of $\lambda_{\mathrm{T,\ U}}^{\mathrm{n}}$ for $k_1a\in[0.01,6],$ and $n\in[1,3,5].$

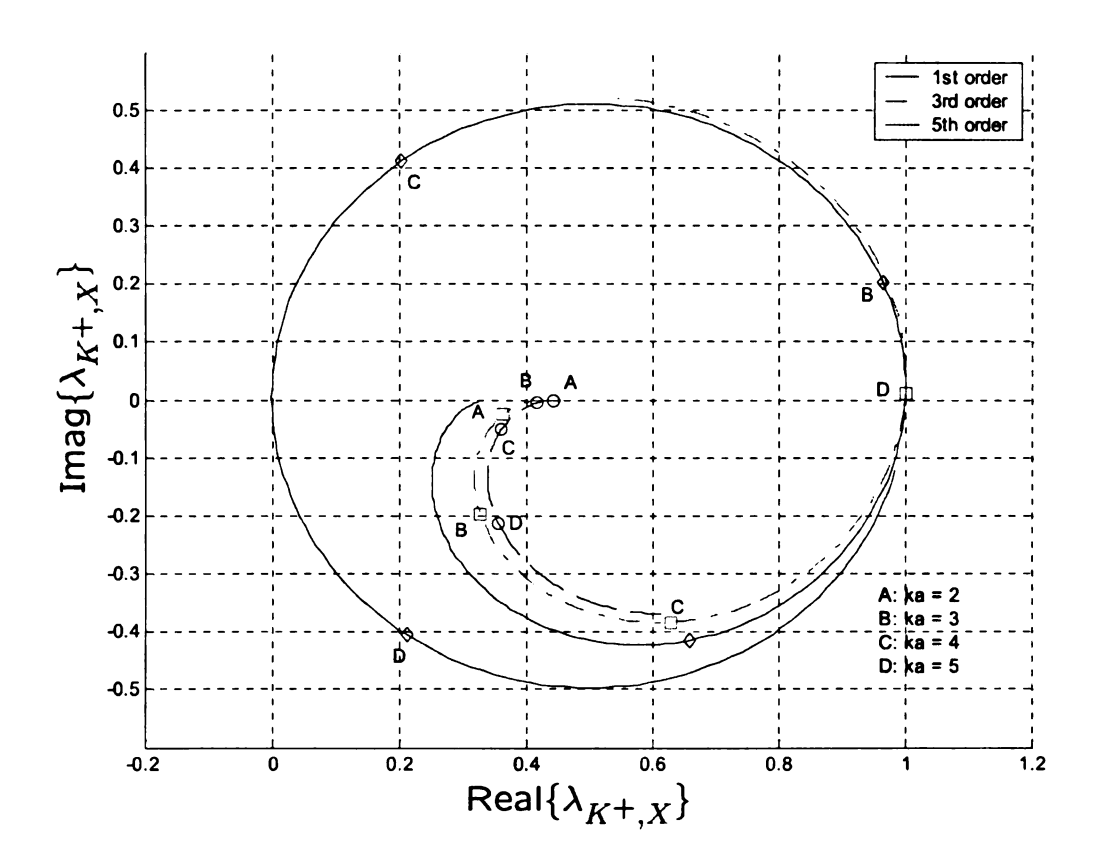


Figure 4.3. Plot of three spectral functions of $\lambda_{K^+,X}^n$ for $k_1a \in [0.01,6]$, and $n \in [1,3,5]$.

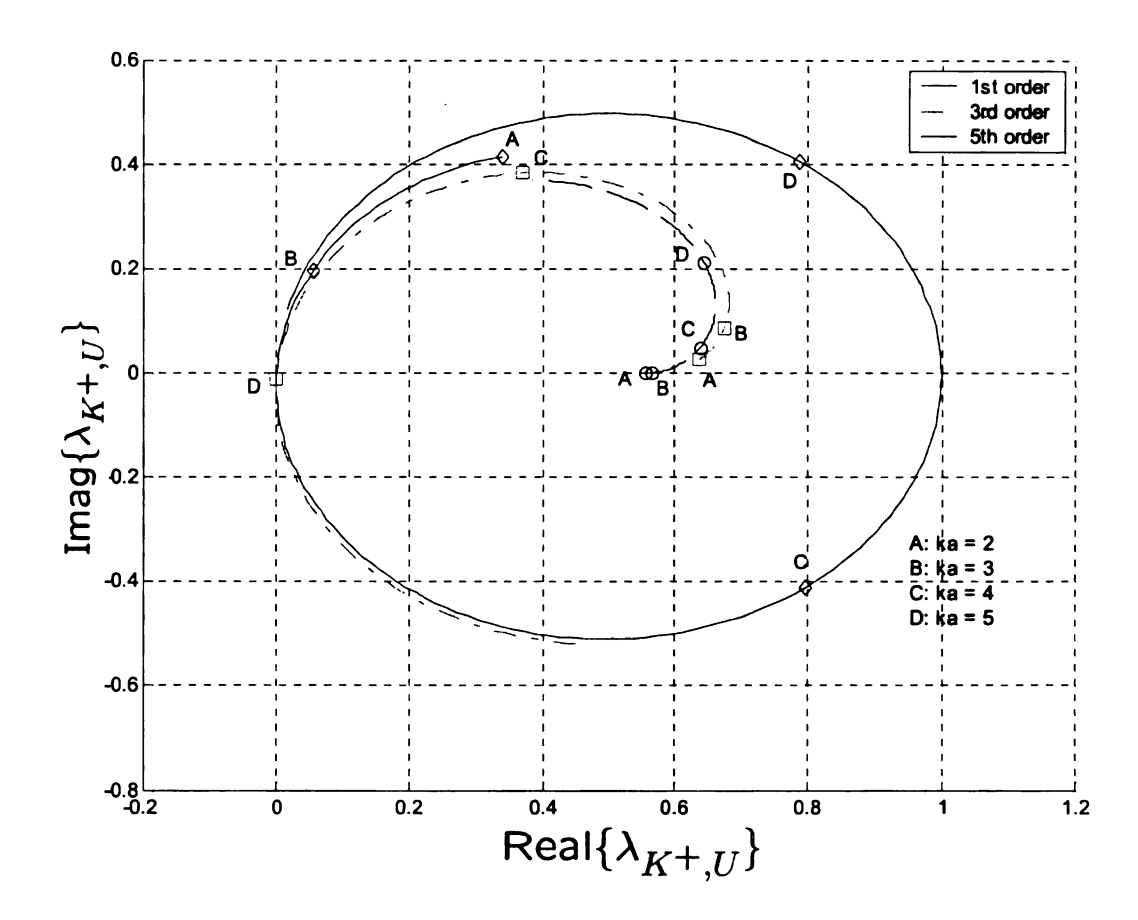


Figure 4.4. Plot of three spectral functions of $\lambda_{K^+,U}^n$ for $k_1a \in [0.01,6]$, and $n \in [1,3,5]$.

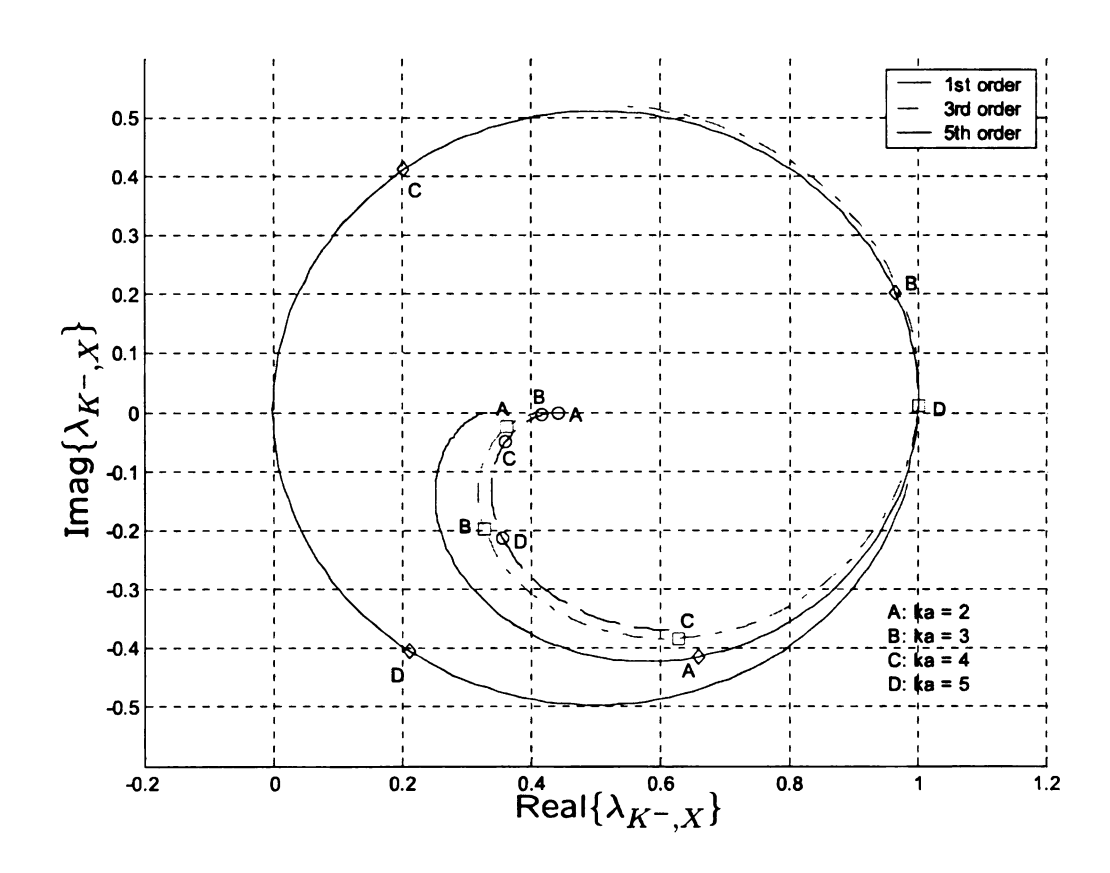


Figure 4.5. Plot of three spectral functions of $\lambda_{K^-,X}^n$ for $k_1a \in [0.01,6]$, and $n \in [1,3,5]$.

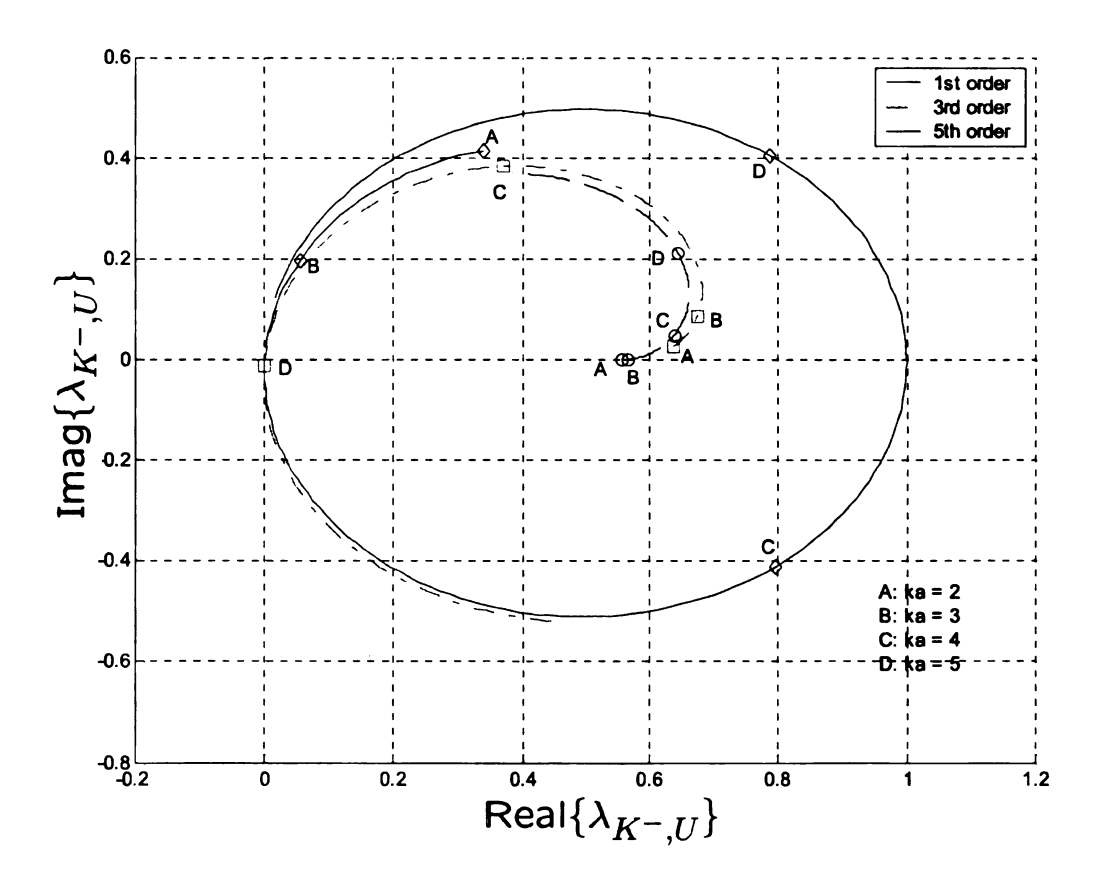


Figure 4.6. Plot of three spectral functions of $\lambda_{\text{K-.U}}^n$ for $k_1a \in [0.01,6]$, and $n \in [1,3,5]$.

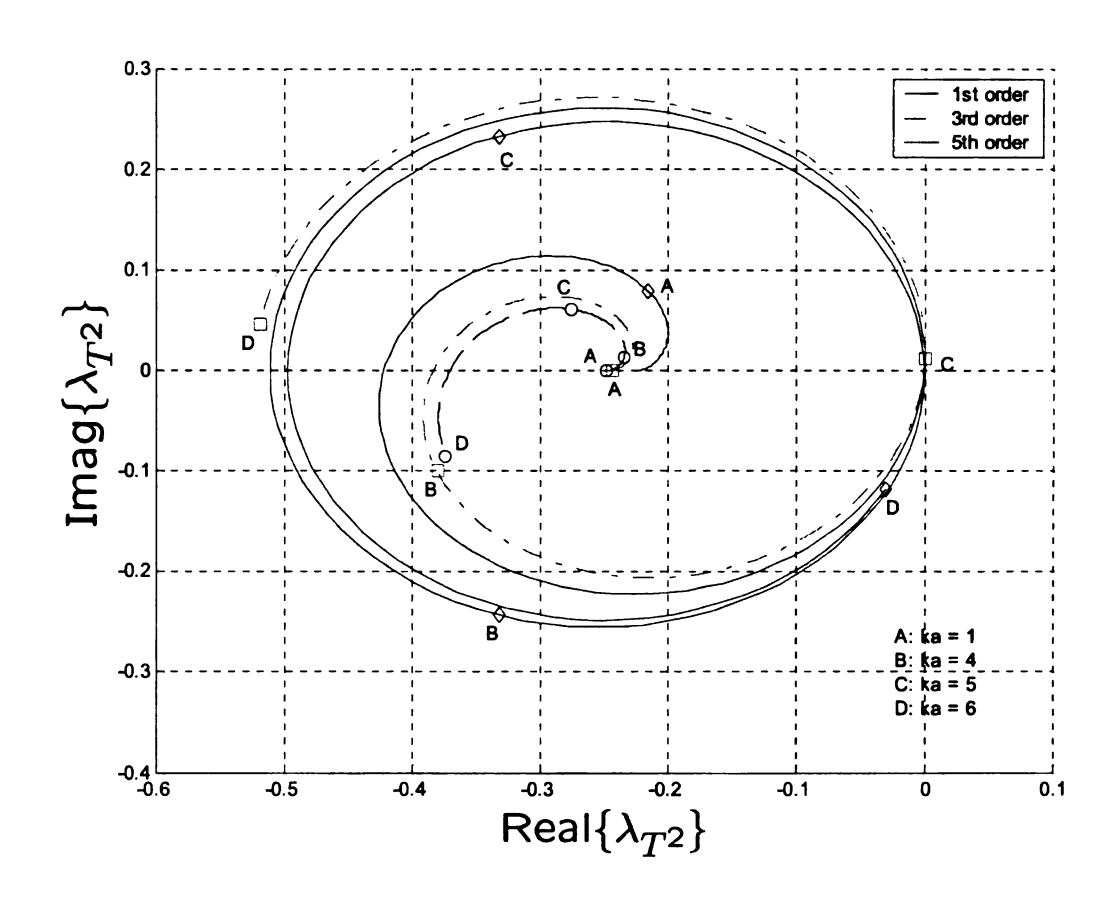


Figure 4.7. Plot of three spectral functions of $\lambda_{\mathrm{T}^2}^{\mathrm{n}}$ for $k_1a \in [0.01, 6]$, and $n \in [1, 3, 5]$.

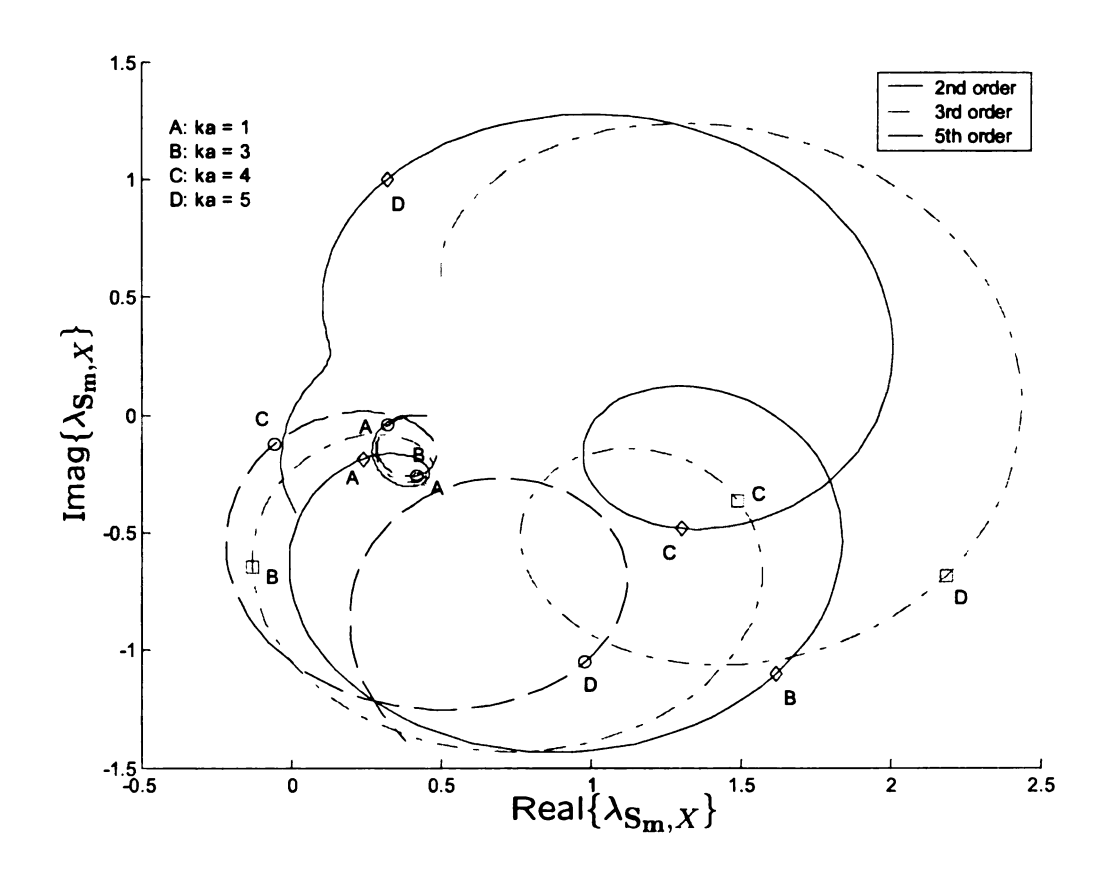


Figure 4.8. Plot of three spectral functions of $\lambda_{\mathbf{Sm}, \mathbf{X}}^{\mathbf{n}}$ for $k_1 a \in [0.01, 6]$, $\frac{\varepsilon_2}{\varepsilon_1} = 4.0$ and $n \in [2, 3, 5]$.

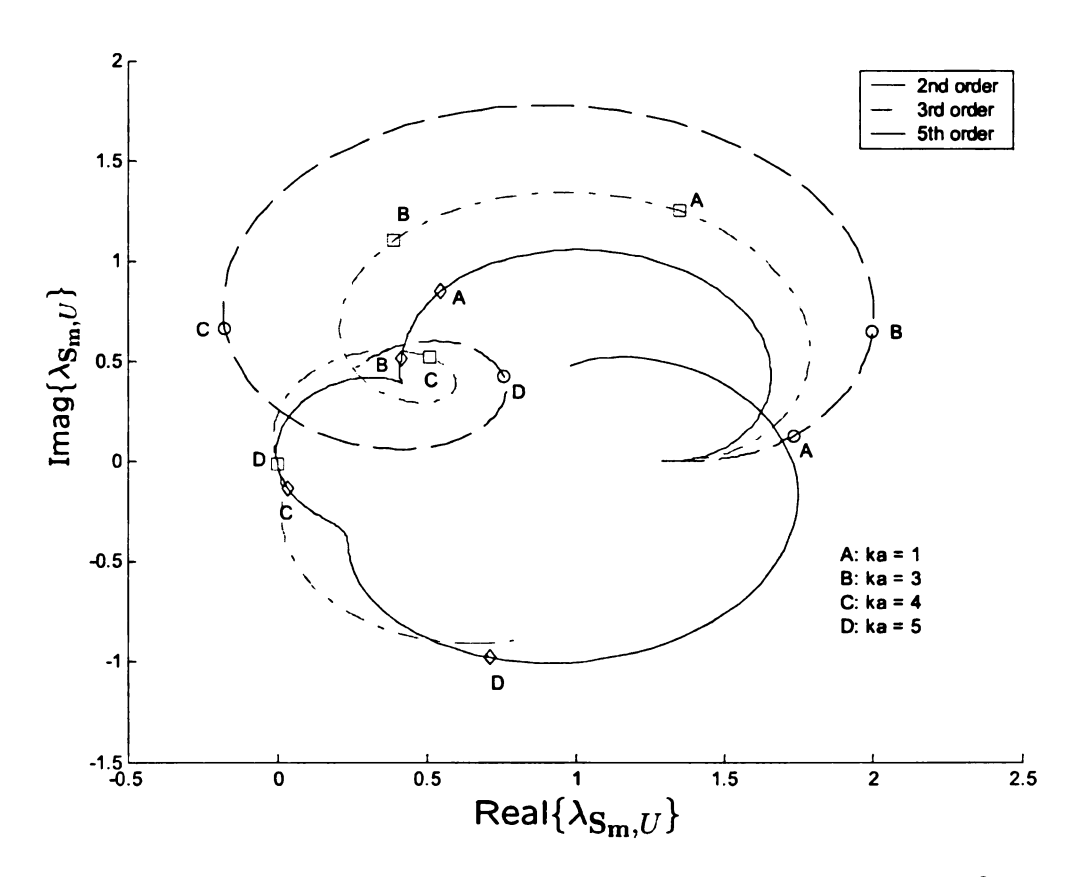


Figure 4.9. Plot of three spectral functions of $\lambda_{\mathbf{Sm},\ \mathbf{U}}^{\mathbf{n}}$ for $k_1a \in [0.01,6], \frac{\varepsilon_2}{\varepsilon_1} = 4.0$ and $n \in [2,3,5].$

CHAPTER 5

CONCLUSIONS

This thesis presented an mathematical perspective of a new integral equation for analyzing the scattering from arbitrary dielectric bodies. The equivalence models, the numerical implementation using MoM, and the rigorous analysis of the spectrum properties of the SIE operator was covered. A modified SIE scheme was devised and proven to be second-kind and resonance free for spheres.

First, the standard models for analyzing the scattering from dielectric objects were introduced, followed by a in-depth discussion of their respective pros and cons. The SIE integral equation, with the subsets of MFIE and EFIE, was presented in detail.

Second, the general method of moments was covered, with the emphasizing on the conventional steps converting a linear integro-differential equation into a matrix equation. The RWG triangular basis function was reviewed, and used to represent the effective unknown current in a discretized form. A two-stage projection technique was specified, i.e., the inner product was defined and two cascaded matrices were constructed to replace the SIE integral equation with a matrix equation. Then the accelerative algorithm, FMM was included to expedite the solving phase. Numerical results generated with various geometries were illustrated, and in comparison with the known data, the accuracy and the convergence of the SIE scheme were clearly demonstrated.

Third, the mathematical foundations of the spectrum analysis were covered, starting with the spherical basis functions. All fundamental integral operators were investigated and their spectrum properties were discussion by showing the spectral curves in the complex plane. Then the same steps were applied to the SIE operator. And it is shown that the SIE operator behaves like a second-kind integral operator, but

suffers from spurious resonances. A supplemental magnetic source turned out to be an appropriate remedy, and would yield a combined-source SIE, which were found to be free from resonances.

The thesis extended to discuss an alternative approach to overcome the interior resonance. In this new approach, the normal fields are included to augmented the original SIE-MFIE equation. Rigorous proof shows that this set of augmented field equations possess a unique solution at all frequencies. Crucial difficulties in practical implementation are examined and necessary information is provided as to solve the whole system.

APPENDICES

APPENDIX A

DEFINITION OF A SECOND KIND INTEGRAL OPERATOR

The standard definition of a second kind integral operator is an operator for the form

$$\lambda I + K \tag{A.1}$$

where λ is a constant, I is the identity, and K is a compact operator. In scattering theory, one encounters operators of the form

$$\lambda_1 P_1 + \lambda_2 P_2 + K \tag{A.2}$$

where λ_1 and λ_2 are constants and P_1 and P_2 are orthogonal projection operators such that

$$P_1 + P_2 = I \tag{A.3}$$

Operators of the form A.2 possess most of the desirable properties of second integral operators. Such expressions are referred as second kind integral operators throughout this paper.

BIBLIOGRAPHY

BIBLIOGRAPHY

- [1] R.F. Harrington, Time-harmonic Electromagnetic Fields, McGraw-Hill, 1961.
- [2] J.R. Mautz and R.F. Harrington, "Electromagnetic scattering from a. homogeneous material body of revolution," AEU, vol. 33, pp. 71C80, Feb. 1979.
- [3] Müller, C. Foundations of the Mathematical Theory of Electromagnetic Waves, Springer-Verlag, 1969
- [4] E. Marx, "Integral equation for scattering by a dielectric," *IEEE Trans. Antennas Propagat.*, vol. 32, pp. 166-172, 1984.
- [5] A. W. Glisson, "An integral equation for electromagnetic scattering from homogeneous dielectric bodies," *IEEE Trans. Antennas Propagat.*, vol. 32, pp. 173-175, Feb. 1984.
- [6] M. S. Yeung, "Single integral equation for electromagnetic scattering by threedimensional homogeneous dielectric objects," *IEEE Trans. Antennas Propagat.*, vol. 47, pp. 1615-1622, Oct. 1999.
- [7] M. Y. Xia, C. H. Chan, S. Q. Li, B. Zhang and L. Tsang, "An efficient algorithm for electromagnetic scattering from rough surface using a single integral equation and the sparse-matrix canonical grid method," *IEEE Trans. Antennas Propagat.*, vol. 51, pp. 1142-1149, Jun. 2003.
- [8] R.F. Harrington, Field Computation by Moment Methods. New York: MacMillan, 1968
- [9] S. M. Rao, D. R. Wilton, and A.W. Glisson, "Electromagnetic scattering by surfaces of arbitrary shape," *IEEE Transactions on Antennas and Propagation*, vol. 30, no. 3, pp. 409-418, May 1982.
- [10] R. Coifman, V. Rokhlin, S. Wandzura, "The Fast Multipole Method for Wave Equation: a Pedestrian Prescription," *IEEE Transactions on Antennas and Propagation*, vol. 35, pp. 7-12, Jun. 1993.
- [11] R.W. Freund, "A transpose-free quasi-minimal residual algorithm for non-Hermitian Linear systems," SIAM J Sci Comput 14 (1993), pp. 470-482.

- [12] Y. Jun, B. Shanker and L. C. Kempel, "Fast multipole augmented analysis of scattering from dielectric objects using the single integral equation," The Applied Computational Electromagnetics Society (ACES) 2004 Conference, Syracuse, NY, Apr. 19-23, 2004.
- [13] G. Mie, "Beitrage zur Optik trüber Medien, speziell kolloidaler Metallösungen," Ann. Phys. vol. 25, pp. 377-445, 1908.
- [14] B. Shanker, A.A. Ergin, M Lu, E. Michielssen, "Fast analysis of transient electromagnetic scattering phenomena using the multilevel plane wave time domain algorithm," *IEEE Transactions on Antennas and Propagation*, vol. 51, pp. 628-641, Mar. 2003.
- [15] G. C. Hsiao and R. E. Kleinman, "Mathematical foundations of error estimates in numerical solutions of integral equations in electromagnetics," *IEEE Trans*actions on Antennas and Propagation, vol. 47, no. 3, pp. 316-328, Mar. 1997.
- [16] M. Abramowitz and I. A. Stegun, "Handbook of mathematical functions," in Applied Mathematics Series. Cambridge, MA: National Bureau of Standards, 1972.
- [17] J. R. Mautz, "A combined-source solution for radiation and scattering from a perfectly conducting body," *IEEE Transactions on Antennas and Propagation*, vol. 27, no. 4, Jul. 1979.
- [18] A. D. Yaghjian, "Augmented electric- and magnetic-field integral equation," Radio Science, vol. 16, no. 6, pp. 987-1001, Nov.-Dec. 1981
- [19] G. Pisharody and D. S. Weile, "Electromagnetic scattering from homogeneous dielectric bodies using time-domain integral equations," *IEEE Transactions on Antennas and Propagation*, vol. 54, no. 2, pp. 687-697, Feb. 2006.
- [20] Mirsky, L., An introduction to Linear Algebra, Oxford University Press, New York, 1955
- [21] R. J. Adams and N. J. Champagne, "A numerical implementation of a modified form of the electric field integral equation," *IEEE Transactions on Antennas and Propagation*, vol. 52, no. 9, pp. 2262-2266, Sep. 2004.
- [22] R. D. Graglia, D. R. Wilton, and A. F. Peterson, "Higher order interpolatory vector bases for computational electromagnetics, *IEEE Transactions on Antennas and Propagation*, vol. 45, pp. 32-342, 1997.

